

Syracuse University

SURFACE

Theses - ALL

5-2015

MULTIPLE GENERATIONS OF FAULTING: A KINEMATIC ANALYSIS OF THE LAGARFLJÓT REGION, NORTHEAST ICELAND

Keegan Runnals
Syracuse University

Follow this and additional works at: <https://surface.syr.edu/thesis>



Part of the [Earth Sciences Commons](#)

Recommended Citation

Runnals, Keegan, "MULTIPLE GENERATIONS OF FAULTING: A KINEMATIC ANALYSIS OF THE LAGARFLJÓT REGION, NORTHEAST ICELAND" (2015). *Theses - ALL*. 114.

<https://surface.syr.edu/thesis/114>

This is brought to you for free and open access by SURFACE. It has been accepted for inclusion in Theses - ALL by an authorized administrator of SURFACE. For more information, please contact surface@syr.edu.

1. Abstract

The North American/Eurasian plate boundary in Iceland is structurally diverse with oblique rifts, volcanic fissure swarms, and transform zones, and a hotspot. Lagarfljót is a lake located in the Tertiary flood basalts of East Iceland, that range in age from ~7 to 3 Ma. The lake is approximately 50 km east of the actively spreading, NS-trending, Northern Rift Zone (NVZ), and occupies a northeast-trending depression in an area of strong NS lineaments. A flexure zone, or zone of steeply dipping lavas, runs N-S across the southern part of the lake, and predates an angular unconformity in the regional lava pile.

A detailed investigation of fault zones in exposures in cliffs along the lakeshore and streams reveal a series of dikes and faults. These dikes and faults can be correlated with the lineaments, and indicate a complicated tectonic history. Fault zones are characterized by fault breccia, cataclasite and gouge with well-developed slickenlines and clear shear-sense indicators. Fault gouge in individual shear zones range in thickness from centimeters to meters. Cross cutting relationships define the relative ages of two families of structures, both post-dating the flexure. The older generation of faults are NS-striking, dextral, strike-slip faults. These are cut by NE-striking, normal faults. The normal faults typically cut existing large dikes or swarms of dikes ranging from 1 – 5 m wide. Displacements along individual normal faults range from centimeters up to 8 m. Some faults cut the lavas above the unconformity and locally rotated structures suggest that limited tilting of the lava pile occurred during faulting. These findings are evaluated with respect to larger scale processes of propagation and relocation of the NVZ.

MULTIPLE GENERATIONS OF FAULTING: A KINEMATIC
ANALYSIS OF THE LAGARFLJÓT REGION, NORTHEAST
ICELAND

By:

Keegan T. Runnals
B.S. Bates College, 2011

Thesis

Submitted in partial fulfillment of the requirements for the degree of Master of
Science in Earth Sciences

Syracuse University
May 2015

Copyright © Keegan T. Runnals

All rights reserved

Acknowledgements

I would like to thank Professor Jeff Karson for taking me on for this project and guiding me in the field and in the department as I completed my M.S. Thanks to my committee members Professor Rob Moucha and Professor Paul Fitzgerald as well as Chris Scholz for their helpful edits and reflections as I went through the writing process. A big thanks to Anthony Fiorentino for his help in the field during the summer of 2015, as well as James Proett who was always behind me to bounce ideas off of. I would like to acknowledge the National Science Foundation who provided the funding to complete two seasons of fieldwork in Iceland. Finally I would like to extend thanks to the entire Syracuse University Earth Science Department, which was a great and supportive place to spend two years getting my degree.

Table of Contents

Abstract	i
Title Page	ii
Copyright	iii
Acknowledgements	iv
Table of Contents	v
List of Figures	vi
List of Tables	vi
Introduction	1
2.1 Tectonic Background	1
2.2 Regional Geology and Previous Work	6
2.3 Lagarfljót Valley	9
Field and Analytical Methods	14
Results	16
4.1 Flexure Zone	18
4.2 Strike-Slip Faulting	20
4.3 Dikes	22
4.4 Normal Faulting	25
4.5 Hafursá River Fault Zone	28
Interpretation	31
5.1 Estimates of net displacement from gouge thickness	35
Discussion	37
6.1 Origin of dikes and normal faults	37
6.2 Origin of strike-slip faulting	40
6.2.1 Bookshelf faulting between adjacent fissure swarms	40
6.2.2 Abandoned Transform Zone	42
6.2.3 Strain partitioning from oblique plate movement	42
6.2.4 Block rotation via a propagating rift	44
Conclusions	47
Appendix	48
References	68
Vita	73

List of Figures

Figure 1. Geologic map showing the lithologies and structures of Iceland.	2
Figure 2. 3D representation of a central volcanic complex in Iceland.	4
Figure 3. Example of bookshelf faulting.	5
Figure 4. Explanations of rift-parallel strike-slip faulting.	7
Figure 5. General depiction of kinematics and heat flow in a volcanic rift zone.	8
Figure 6. Compiled ages in Ma of lavas and dikes in the Lagarfljót region.	9
Figure 7. Map of study area with measured dips of lava's.	11
Figure 8. Photo of angular unconformity.	12
Figure 9. Photo of sedimentary unconformity.	12
Figure 10. Graphical example of slip line analysis.	15
Figure 11. Map of study area showing major structures.	17
Figure 12. Photograph showing a dike cutting a strike-slip fault zone.	18
Figure 13. Deformation associated with flexure zone.	19
Figure 14. Stereonet showing strike-slip fault planes.	20
Figure 15. Strike-slip features seen in the field.	21
Figure 16. Histogram of dike widths.	22
Figure 17. Map displaying orientation and thickness of dikes.	23
Figure 18. Stereonets and rose plots showing orientations of dikes and faults.	24
Figure 19. Stereonet showing normal fault planes.	25
Figure 20. Normal fault kinematic features.	26
Figure 21. Large normal fault zone found in the Klifá river.	27
Figure 22. Hafursá River location, with interpreted structures.	29
Figure 23. Focal mechanisms produced from all faults in field area	33
Figure 24. Focal mechanisms produced from Hafursá fault zone.	34
Figure 25. Log-log plot of fault gouge thickness vs. fault displacement.	36
Figure 26. Model for the development of the Lagarfljót region.	38
Figure 27. Cross-sectional view showing basaltic flows and unconformity.	39
Figure 28. Schematic showing how throw can be estimated for one fault.	40
Figure 29. Schematic for strike-slip faulting proposed between fissure swarms.	41
Figure 30. Schematic showing transform hypothesis in Lagarfljót region.	42
Figure 31. Strain partitioning in Lagarfljót region.	43
Figure 32. Propagating rift hypothesis.	45

List of Tables

Table 1. Inferred geologic events of the Lagarfljót Lake study region through time.	34
--	----

2. Introduction

2.1 Tectonic Background

Iceland is a broad crustal platform of thick oceanic crust, situated above a hotspot. It is divided between the American and Eurasian plates, with this boundary manifest offshore as the Mid-Atlantic Ridge (MAR) (Figure 1). Spreading at the current boundary has persisted for at least two million years at a rate of 18.2 mm/yr and direction of N105°E (DeMets et al., 1994; Einarsson, 2008). The hotspot strongly influences the geometry of the plate boundary in Iceland (Figure 1). The geometry of spreading is complicated by the occurrence of ridge jumps, propagating rifts, and migrating transforms (LaFemina et al., 2005; Einarsson, 2008; Karson, 2013).

As the Reykjanes Ridge approaches Iceland it spreads obliquely, continuing onshore into the Reykjanes Peninsula. The spreading direction here is oriented approximately 30° counterclockwise from orthogonal to the plate boundary. This segment of the boundary is defined by a series of *en echelon* volcanic shields and fissure swarms that are cut by normal faults, eruptive, and non-eruptive fissures. These structures are defined by parallel dikes, normal faults, and fissures, and are mostly active during magmatic episodes that occur roughly every 1000 years (Einarsson, 2008) (Figure 2). There is evidence of low magnitude strike-slip motion that accommodates oblique spreading in these zones during “dry” periods of low magma output on the peninsula (Clifton & Kattenhorn, 2006; Einarsson, 2008).

As the plate boundary continues north through the peninsula it splits at the Hengill Triple Junction (Figure 1). The northwest segment is the Western Volcanic Zone (WVZ), which has been shown to be part of a dying rift zone (LaFemina et al., 2005). The eastern segment is a right-stepping transform zone termed the South Icelandic Seismic Zone (SISZ), which connects the Reykjanes Ridge to the Eastern Volcanic Zone (EVZ). The SISZ consists of a series of N-S dextral strike-slip bookshelf faults that accommodate displacement across an overall left-lateral transform zone (Einarsson, 1991).

The EVZ continues north through the center of the hotspot, located under the northwest

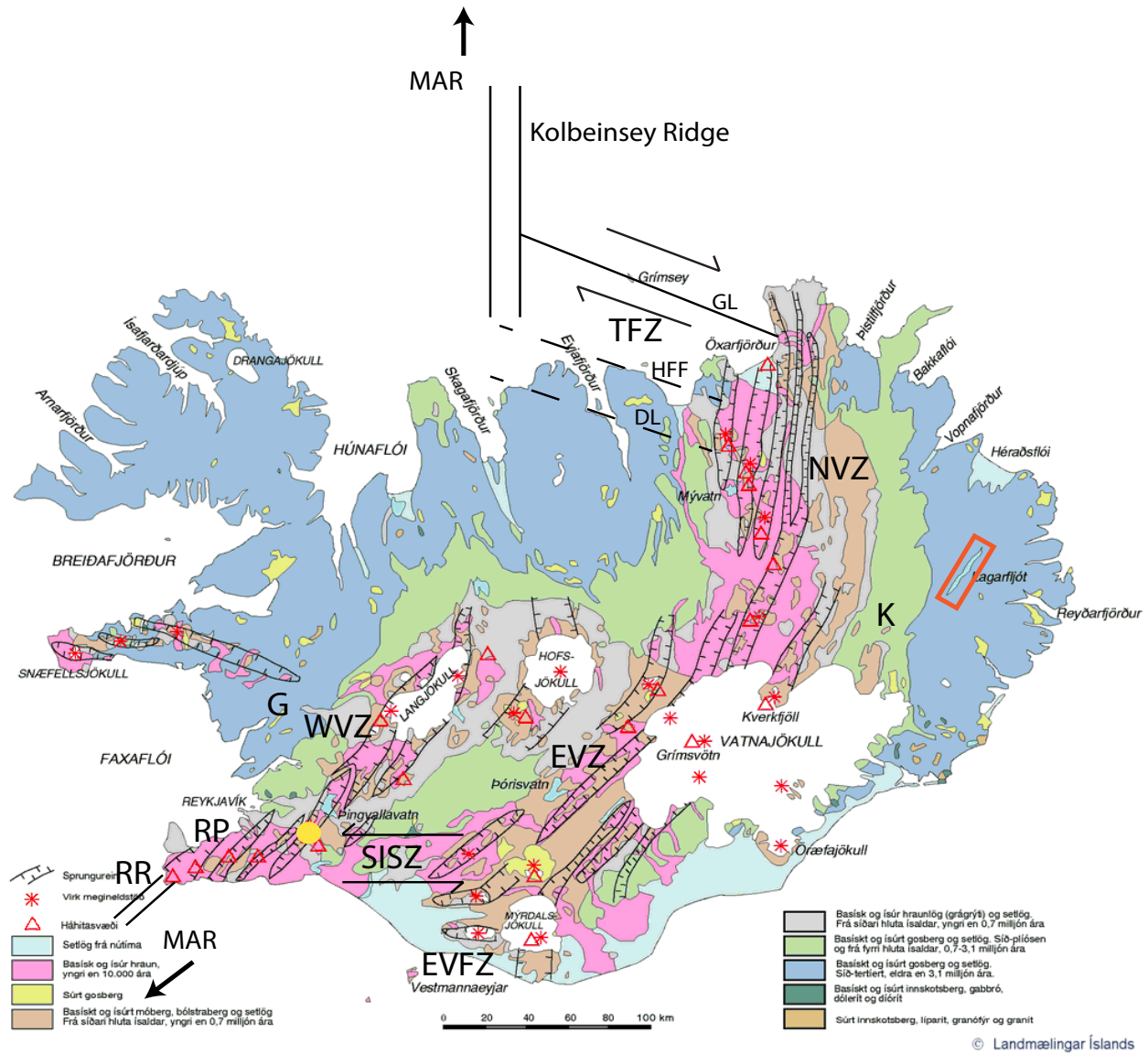


Figure 1. Geologic map showing the lithologies and structures of Iceland. Red triangles are central volcanoes, with black hashed lines indicating the rift zones. Yellow dot in southwest signifies the Hengill Triple Junction. Labeled segments are as follows: Mid-Atlantic Ridge (MAR), Reykjanes Ridge (RR), Reykjanes Peninsula (RP), Western Volcanic Zone (WVZ), South Icelandic Seismic Zone (SISZ), Eastern Volcanic Flank Zone (EVFZ), Eastern Volcanic Zone (EVZ), Northern Volcanic Zone (NVZ), Tjornes Fracture Zone (TFZ), Grimsey Lineament (GL), Husavik-Flatey Fault (HFF), Dalvik Lineament (DL), Kárahnjúkur (K), Gljúfurá (G). Orange box indicates the area of this study. Modified from (Jóhannesson & Sæmundsson, 2009)

portion of the Vatnajökull ice cap, and connects to the Northern Volcanic Zone (NVZ) (Figure 1). These portions of the rift are defined by active N-S fissure swarms that are each associated with a central volcano along the ridge axis (Figure 1). The NVZ then links to the Kolbeinsey Ridge through the Tjornes Fracture Zone (TFZ), which is made up of a series of left-stepping transform zones (Figure 3) oriented WNW-ESE (Saemundsson, 1974). This succession of transform zones is thought to accommodate the northwards propagation of the NVZ, and is evident in seismicity data (Einarsson, 2008). There are thought to be three of these transverse zones, with the northernmost concentrating the majority of present day seismicity and the southernmost the least. Transform zones bound crustal blocks made up of NNE-SSW-striking faults that have a left-lateral sense of motion (Figure 1).

The spatial and temporal evolution of the plate boundary zone across Iceland is an issue that is still debated. Evidence for eastward ridge jumps accommodating westward movement of the MAR relative to the hotspot is inferred from geochemical and structural data (Einarsson, 1991; Hardarson, 1997; Marin et al., 2011). At least three paleo-rift segments with life spans of ~8 million years have been proposed in NW Iceland, Snaefellsnes, and Skagafjörður (Hardarson, 1997, Garcia et al., 2003). Recent geodetic work has shown that spreading is currently being transferred from the dying WVZ to the EVZ in southern Iceland (Lafemina, 2005; Arnadóttir, 2009). This work also provides evidence for southwest propagation of the EVZ segment into the EVFZ (Figure 1). Along-strike variation in the spreading rate can be observed in the EVZ as well, decreasing from 15 mm/yr in the northeast to 9 mm/yr in the southwest (Lafemina et al., 2005). Though there have not been any similar studies done in the NVZ, a similar process can be assumed to be occurring.

Iceland has traditionally been assumed to generally accommodate plate divergence through normal faulting and fissuring related to tectonic extension (Einarsson, 2008). Strike-slip faulting in Iceland is prevalent, but mainly associated with transform zones or oblique-spreading segments. The SISZ and TFZ have been well studied through instrumentation, with focal mechanisms indicating lateral movement along parallel, transverse faults (Einarsson, 1991).

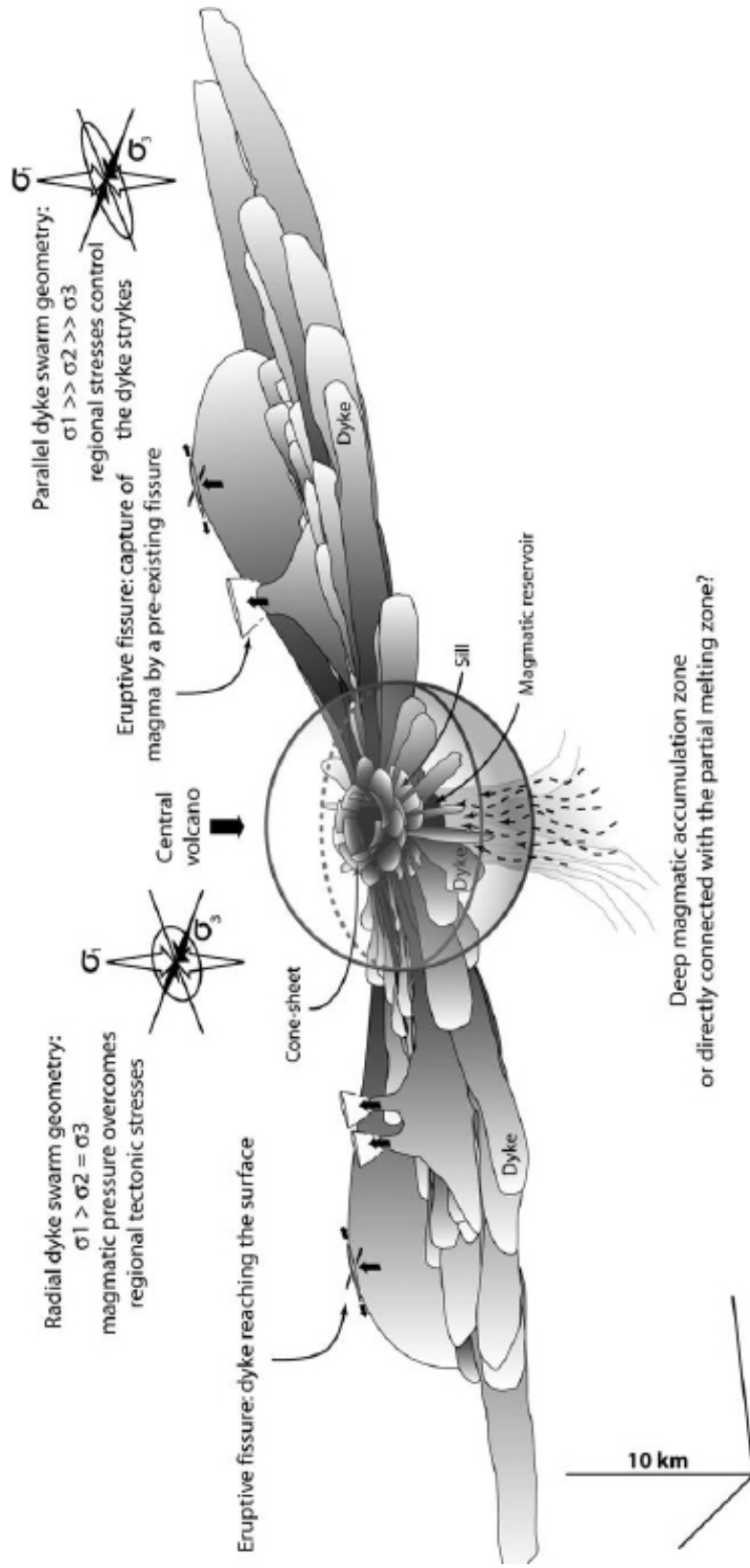


Figure 2. 3D representation of a central volcanic complex in Iceland, such as those found in the neovolcanic zone. Dikes are shown to radiate out laterally from a central reservoir or volcano. The strikes of the propagating dikes vary depending on the local stress conditions. Some dikes will propagate vertically to the surface, resulting in an eruptive fissure such as those seen during the Krafla rifting episode. σ_3 is the dominant stress in the region, and controls local dike orientations. (From Paquet et al., 2007).

Small-scale strike-slip indicators have also been observed in oblique rift segments, usually manifested as small push-up or pull-apart structures such as those found on the Reykjanes Peninsula (Clifton & Kattenhorn, 2006). Bookshelf-type faulting has also been observed locally to accommodate the transfer of motion between the en-echelon Askja and Kverkfjöll segments of the NVZ. Approximately five blocks 15 by 2 km are inferred to have been rotated 15° over a 0.4 - 0.8 Myr timescale. This gives a slip rate of 0.9-1.8 mm/yr along each fault (Green et al., 2013).

However, enigmatic rift-parallel strike-slip faults outside of any transform zone or highly oblique rift segments are present. A paper by Passerini et al. (1997) was the first to consider these structures in detail. In it, the authors described their observations of common rift-parallel strike-slip faults that were found in western, south-central, and south-eastern Iceland. The Lagarfljót Valley is specifically mentioned as a location that contains abundant strike-slip and normal faulting. They suggest three possible modes of formation for these types of faults in southern

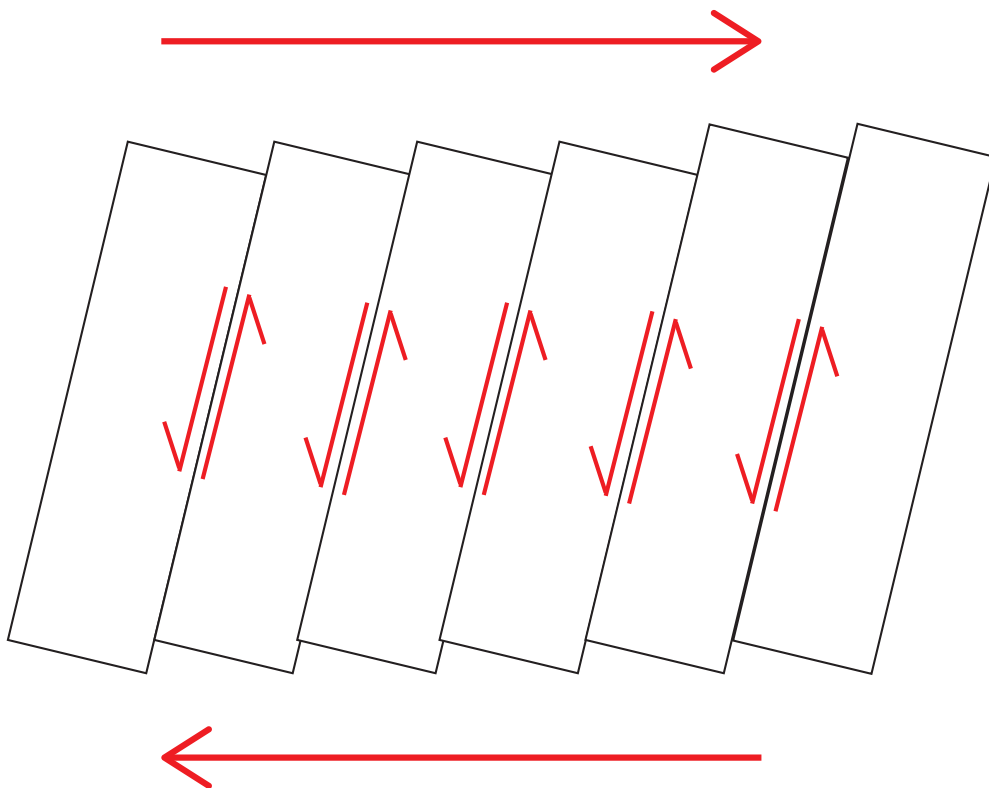


Figure 3. Example of bookshelf faulting; sinistral strike-slip faults accommodate an overall right-lateral transform zone. This is observed in the Tjornes Fracture Zone of Northern Iceland (Einarsson, 2008).

Iceland which are outlined in Figure 4.

More recent studies in Kárahnjúkar (Chutas et al., 2006) and Gljúfurá (Nanfito & Karson, 2009) are isolated examples of rift-parallel strike-slip faults unrelated to transform offsets, with displacements inferred to be orders of magnitude greater than those seen in the transform zones. Continued work has identified rift-parallel strike-slip faults in Sauðárarkrókur and Akureyri (Karson, personal communication, 2014).

2.2 Regional Geology and Previous Work

Lagarfljót is a 60-km-long lake in the Tertiary volcanic terrane of Eastern Iceland. The area is located about 80 km east of the active NVZ segment (Figure 1). The exposed lava pile in Eastern Iceland is 9 km thick, and composed of about 80% tholeiites and olivine tholeiites (Kristjánsson & Gudmundsson, 2005). Acid and intermediate rocks account for ~10% of the section, and inter-bedded sedimentary rocks account for the remaining 5-10% of the stratigraphy. Walker (1958) showed that lava flows in the east tend to dip westwards (towards the rift axis), possibly because of loading by new crust in the NVZ. Westward dips of the lava beds steadily increase from 2° at the highest elevations to 9° at sea level, with higher dips seen locally.

Ages of the rocks in the vicinity of Lagarfljót are poorly constrained, with only one dike being dated to 8.8 ± 0.2 Ma using the K-Ar method (Figure 6) (Garcia et al., 2003). A sedimentary package dipping 10° runs N-S along the east coast. It consists of several hundred meters of fluvial, tuff, and agglomerate sediments overlying lavas that have been tilted up to 25° creating an angular unconformity (Saemundsson, 1974). Geological transects just to the southwest of the unconformity show lava ages ranging from 7 Ma at the bottom of the exposure to 3 Ma at the top (Kristjánsson & Gudmundsson, 2005). Profiles studied to the east by Watkins and Walker (1977) in Mjóifjörður show lavas that are 12 Ma at the base of the exposed lava pile and 9 Ma at the top. They further infer volcanic production rates (based on stratigraphic thickness) that are separated into three episodes. The first episode stretched from 13.4 to 7.6 Ma, with an extrusion rate of ~720 m/myr. The second episode was from 7.6 to 6.5 Ma with

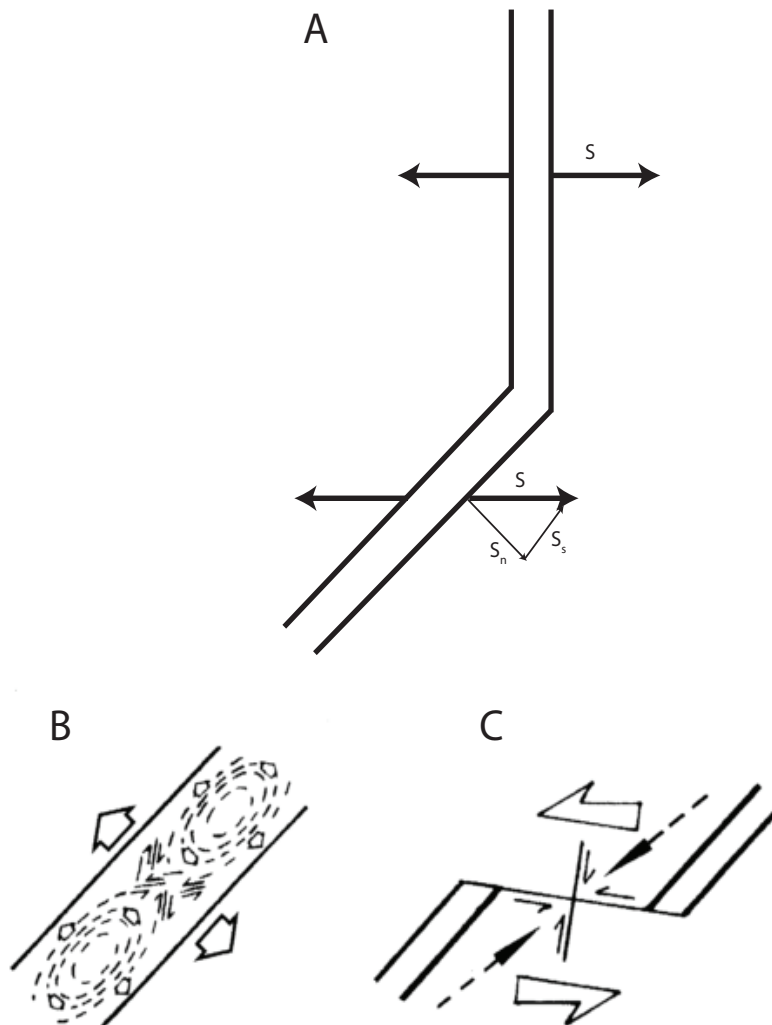


Figure 4. Explanations of rift-parallel strike-slip faulting proposed by Passerini et al. (1997) A) Local rift segments that are oriented oblique to the spreading direction can have normal and strike-slip components. S is the overall spreading direction, with S_n and S_s the normal and strike-slip partitioned components of the oblique segment respectively. B) Local differences in mantle upwelling along a slow-spreading plate boundary can lead to axial compression, where material would flow out of sections with excess supply and converge in sections with insufficient supply. C) Rift-parallel compression is caused by transform shear between adjacent segments, equivalent to R and R' shears. (From Passerini et al. 1997).

an extrusion rate of ~2600 m/myr. The final episode was from 6.5 to 2.3 Ma with much lower extrusion rates of ~360 m/myr. Based on these rates, the location of the study area, and the one dike that was dated; the lavas of the study area are likely in the range of 7-11 Ma. Multiple populations of basaltic dikes cross-cut these lavas indicating a more recent period of volcanism.

Faulting in the region was described briefly by Walker (1974) as a structural complexity related to tilting of the lava pile in what was termed the Lagarfljót Flexure Zone. Flexure zones are common in Iceland, and are identified by lavas that tilt between 5 and 10 degrees. The Lagarfljót Flexure Zone was described as more complicated though, with steeper dips, high-density faulting, and synclinal structures (Walker, 1974; Watkins & Walker, 1977). Saemundsson (1974) suggested that this flexure zone is part of a larger N-S flexure zone found in eastern Iceland. He related it to the initiation of the present day northern rift segment, where rifting began with a series of troughs that quickly filled in with thick sediments. Flexure zones are found across Iceland and delineate present and past rift segments (Figure 5).

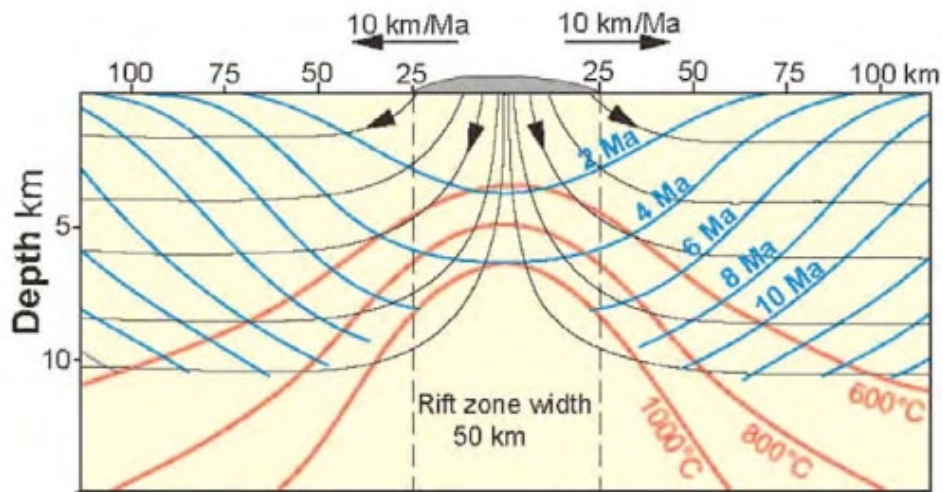


Figure 5. General depiction of kinematics and heat flow in a volcanic rift zone based on the Palmason model (1973). The black lines show mass trajectories with age (blue) and red (temperature) contours overlain. Rapid subsidence occurs at the center of the rift due to thickening of the crust, and results in flexure zones (From Nanfity, 2008).

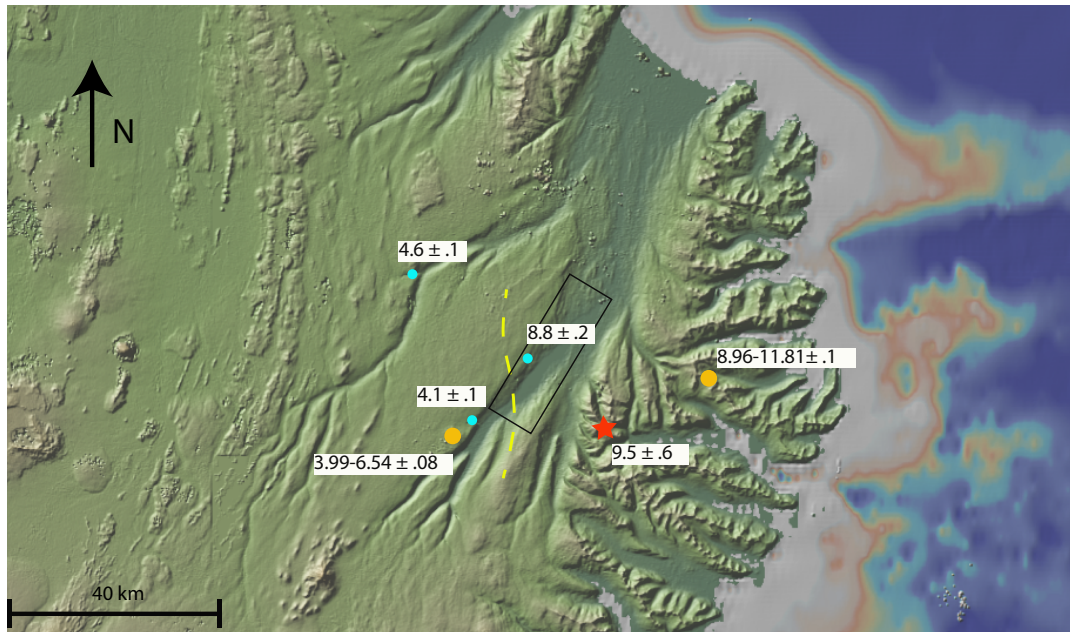


Figure 6. Compiled ages in Ma of lavas and dikes in the Lagarfljót region. All of these samples were dated using K-Ar. Red star is andesite from Moorbath et al., 1968. Orange dots are vertical profiles made along valley walls from McDougall et al., 1976a&b. Blue dots are dikes from Garcia et al., 2003. Yellow dotted line denotes the approximate angular unconformity in the area and the black box indicates Lagarfljót. Map created using GeoMapApp (Ryan et al., 2009)

Few studies have been conducted in the Lagarfljót area since the late 1970's, and the observed strike-slip component suggests that the deformation here is more complex than a simple flexure zone or orthogonal spreading model allows. Kristjánsson and Gudmundsson (2005) compiled previously unpublished structural and paleomagnetic data from the Fljótisdalur valley to the southwest of Lagarfljót. The study looks primarily at the lava sequences and resultant polarity column. However, they briefly mention the presence of a subvertical dike and fault system striking N-NNE. Over 100 faults have been mapped in this area, with fault zones typically 1-5 m wide. In this study 60 dikes were located, typically with a width of 3-5 m but some were up to 10 m wide. They report finding thin zones of fault breccia along the dikes as well. These structures are typical of the Lagarfljót region to the north, though much more abundant in the latter.

2.3 Lagarfljót Valley

The Lagarfljót area is characterized by N-S trending lineaments, and is located just north of the Thingmuli Central Volcano (Figure 6). Andesite erupted from the volcano has been dated

to 9.5 ± 0.6 Ma using the K-Ar method (Moorbath et al., 1968). Thingmuli is the northernmost volcanic complex in a string of en-echelon N-S-trending extinct volcanic centers, and it is suggested that this region of Eastern Iceland sat within the rift zone when these centers were active (Carmichael, 1964; Oskarsson & Riishuus, 2014). As the active spreading center migrated westward, the lavas are inferred to have been tilted in that direction as the upper crust was loaded with newly erupted material (Helgason, 1984). Numerous tholeiitic dikes cut the Tertiary lavas, likely originating from Thingmuli and other neovolcanic centers (Walker, 1964).

Tholeiitic lavas comprise the majority of bedrock in the area, with inter-layered sedimentary beds usually 1-3 m thick. Lavas found in the region are dipping $5-10^\circ$ to the west outside of the flexure zone (Figure 7). Lavas dipping to the south are observed in the northeastern end of the lake, and have been attributed to loading around the Thingmuli volcanic complex. Two samples of lava flows were collected and examined in thin section. Phenocrysts are almost exclusively plagioclase and clinopyroxene, with olivine observed in one of the samples. In many cases the plagioclase had been weathered to produce clay minerals. The compositions confirm earlier studies that indicate lava flows are primarily tholeiites and olivine tholeiites. Orientations of the lavas are N-S striking with dips ranging from 5° to 25° west (Figure 7). The flexure zone is defined by lavas that are dipping $>10^\circ$, and locally eastward dipping lavas are observed within it. The western boundary of this flexure zone is easily observed from the eastern side of the lake (Figure 8).

A 200-300 m thick sedimentary section unconformably overlies the tilted lavas in exposures along river cuts in the western Lagarfljót Valley walls (Figure 9). This unconformity was not observed on the eastern side, but based on the dip of the unconformity and the distance to the eastern valley wall it has likely been eroded away.

Cliffs along the shoreline of Lagarfljót, oriented NE-SW, provide an excellent cross section of these N-S lineaments and dikes in cross section. Fault zones are well exposed along the shore of the lake and in stream cuts along nearby valley walls. Outcrops are weathered and poorly exposed or covered by moss and lichens inland. Fault zones are exposed along the

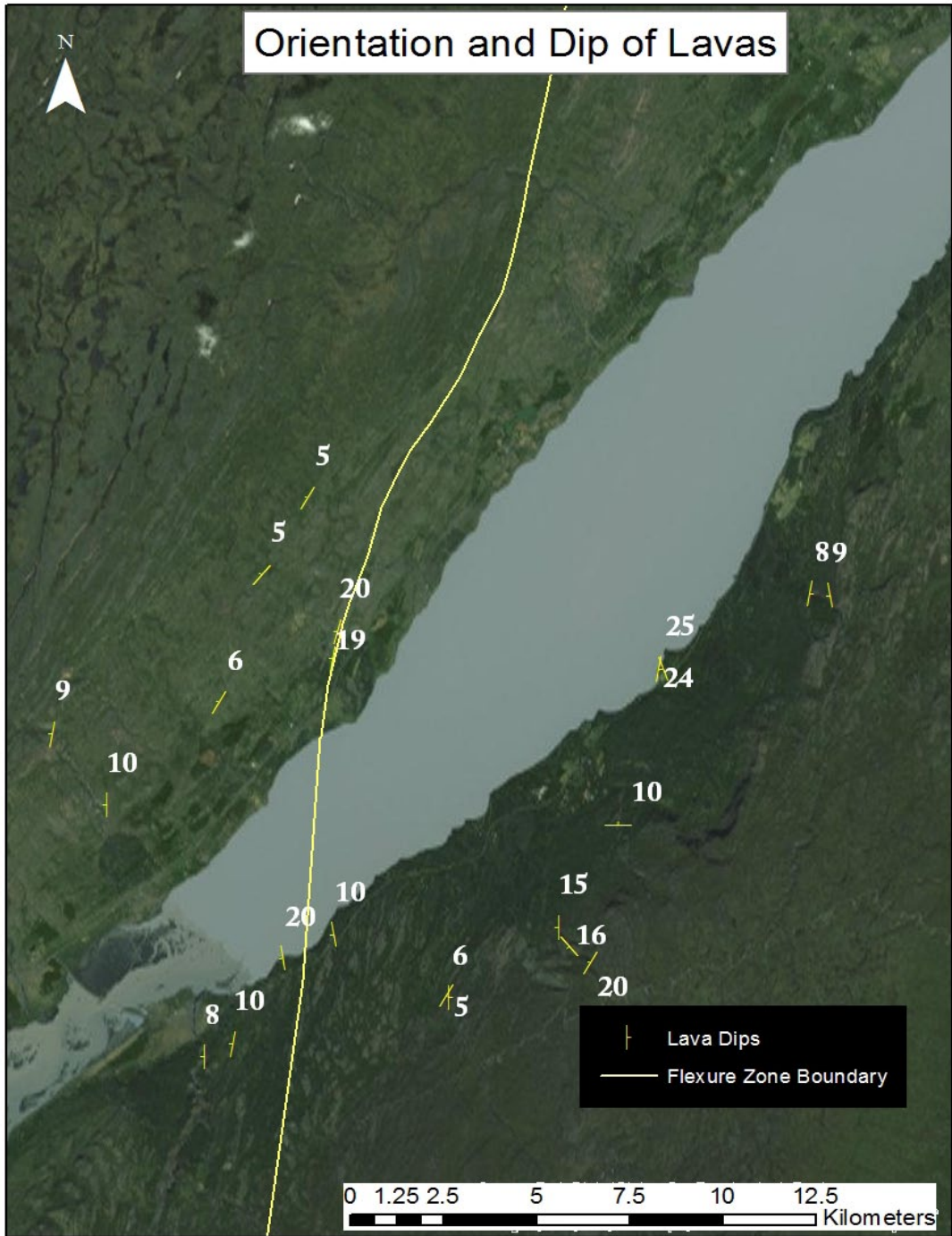


Figure 7. Map of study area with measured dips of lava's. Yellow line delineate the western boundary of the flexure zone containing higher than average dips.



Figure 8. Photo taken from east side of lake looking NW at the angular unconformity that defines the Lagarfljót flexure zone. Lavas below yellow line are dipping 20° W while lavas above are dipping 5° W.



Figure 9. Photo showing sedimentary package seen in the southwestern valley wall of Lagarfljót. Undeformed lavas dipping 9° to the west cap a sedimentary sequence >20 meters thick. Below the unconformity and not visible in the picture are lavas dipping up to 25°. Yellow line denotes the top of the unconformity. Photo taken looking NW.

entire ~60 km length of the lake. The deformation associated with faulting is not distributed consistently, with areas in the southern end of the lake displaying the most intense deformation. The dominant N-S and NE-SW fault zones typically have steeply plunging striations indicative of normal movement. There is also a significant population of fault surfaces that have gently plunging striations, indicative of strike-slip movement. Fault gouge, on the order of a few centimeters to more than one meter thick, defines discrete faults within fault zones that themselves are tens of meters wide and can be traced over 100 m along strike in some places. Fault gouge is also observed within or along the margins of many N-S and NE-SW dikes, indicating post-emplacement deformation. No faults were observed to be cut by the dikes, again indicating deformation events occurred post-emplacement.

Dikes found in the region range from 10 cm wide up to 8 m, with most falling in the 1-3 m range. Cross-cutting relationships seen in multiple places indicate that there have been a series of injections in this region. The majority of normal faulting is found in and along dike margins, indicating post-emplacement deformation. These faults zones are defined by breccia and gouge that range from centimeters up to a meter wide. Some of the largest normal faults are found in deformation zones that span 10's of meters. A thorough kinematic analysis of these structures provides insight into the tectonic deformation that has affected this region of Iceland, as well as contributes to the understanding of the evolution of oceanic crust in similar settings.

3. Field and Analytical Methods

A 60 km x 5 km-wide zone was investigated around Lake Lagarfljót, with a concentration in the southeast corner (Figure 6). The best and most easily accessible exposures are located here in river cuts along the wall of the fjord. A 30-km-long transect was also made north to south across the eastern shoreline, investigating outcrops in exposed cliffs. Aerial and topographic maps were used to determine areas of interest, which were predominately N-S trending river cuts. The western shore was harder to gain access to due to a large agricultural presence there. GPS waypoints were used to mark the coordinates of measurements and structures.

Detailed data collected for selected fault zones include strike and dip of fault planes, rake of slickenlines, strike and dip of dikes, width of dikes, sense of slip on fault, width of fault zone, description of fault gouge, offset of bedding, and any other details pertinent to the outcrop. Sense of slip was determined using small-scale shear fractures (Petit, 1987). Some units were vertically offset across faults, with slickenlines present. With this information sense of shear (SOS) and displacement cant be determined. Striae were recorded using the Aki-Richards format for planes with a clear sense of shear, otherwise a rake was recorded (Allmendinger et al., 1989). Samples of the representative lava units, dikes, and fault gouge were collected for subsequent analysis in hand sample and in thin section. Regional characteristics such as dips of lavas, large-scale lineaments, and other terrain elements were also recorded.

ArcGIS software was used to create maps showing locations of the different structures and their relationships, as well as an overall geologic map of the area. In order to evaluate fault displacements and strain, focal mechanisms (analogous to earthquake focal mechanisms- Marrett & Allmendinger, 1990) for the proposed region and sub-regions were created. Stereonet software was used to plot planes and display orientations of faults and dikes by inputting strike, dip and dip directions (Allmendinger, 2012). FaultKin software (Allmendinger, 2012) was used to solve for the axes of extension (T) and shortening (P), which aid in finding the principal directions of strain in the region (Figure 10). This was done by inputting strike, dip, dip direction, rake, and SOS. The axes were then contoured using the Kamb method (Kamb, 1959) to get principal

directions of strain for the whole data set.

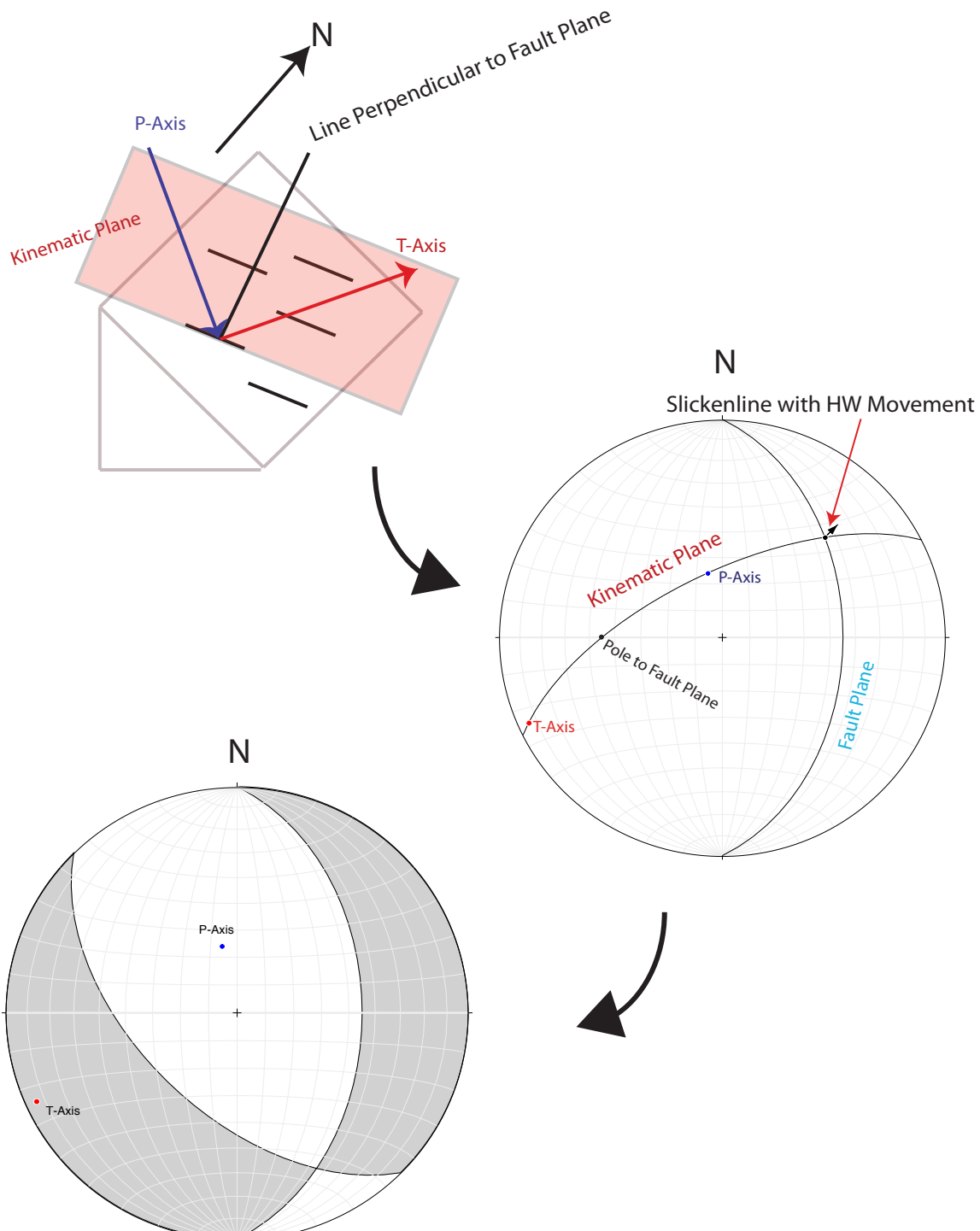


Figure 10. Graphical example of slip line analysis. The kinematic plane is defined by the pole to the plane and the slickenlines. The P & T axes lie within the kinematic plane, 45° in either direction from the pole, with the slip direction indicating the T-axis. The orientation of the fault plane is needed to separate it from the nodal plane in the final result. In this example a N-S striking normal fault with a left-lateral component is presented. This example is for a single fault. With many faults the P & T data points are contoured and best fit axes are determined.

4. Results

Structures found across the study area all generally displayed a NNE trend, with near vertical dips (Figure 11). There are several instances of dikes and faults that fall outside of this trend. The faulting appears to increase moving north to south along the lake, with areas in the south displaying much higher densities of faults than areas in the north. Fault gouge thickness also increases to the south. The southeastern corner of the study area is the easiest to access and has the best exposures within river cuts along the valley walls and exposures along the lake shore. The northern end of the lake consists mostly of highly weathered flood basalts and dikes that sit in flatter outcrops with no river exposures. Faults are hard to distinguish here, and kinematic indicators have been subjected to significant weathering.

Strike-slip fault planes are observed mainly in the southeastern end of the lake, with low-plunge slickenlines and Riedel shears indicating primarily right-lateral movement. These faults trend N-S and in some cases NW-SE. The fault zones are found in and around river-cuts that are trending N-S, and in many cases are cut by NE-SW trending dikes and normal faults. There is no observed offset of dike margins cutting these faults, indicating the faults haven't been active since the dike injections (Figure 12).

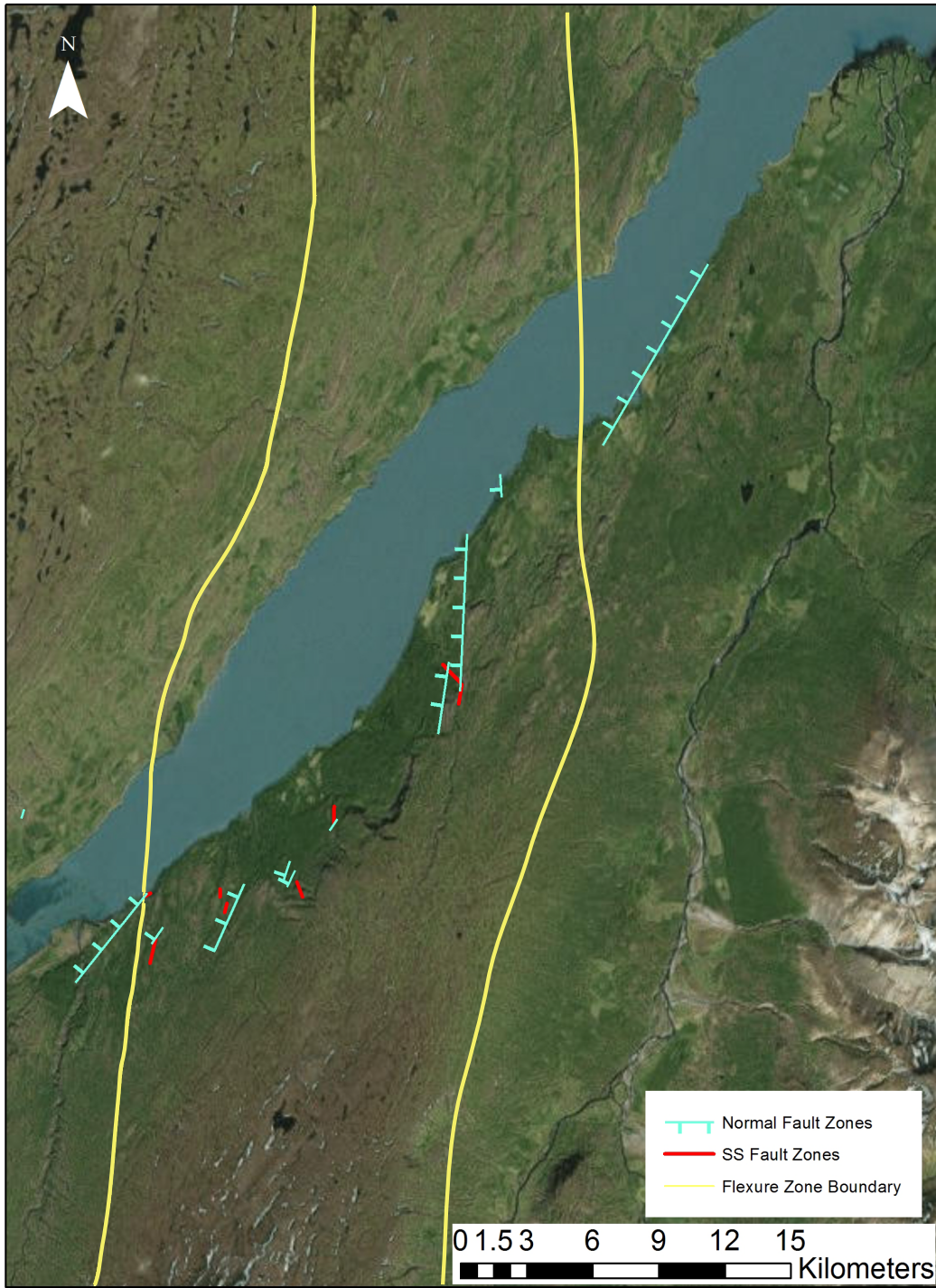


Figure 11. Map of study area showing major structures, which are exclusively in the southern half of the lake. NE-SW trending normal faults cut N-S trending strike-slip faults. Yellow lines delineate flexure zone.

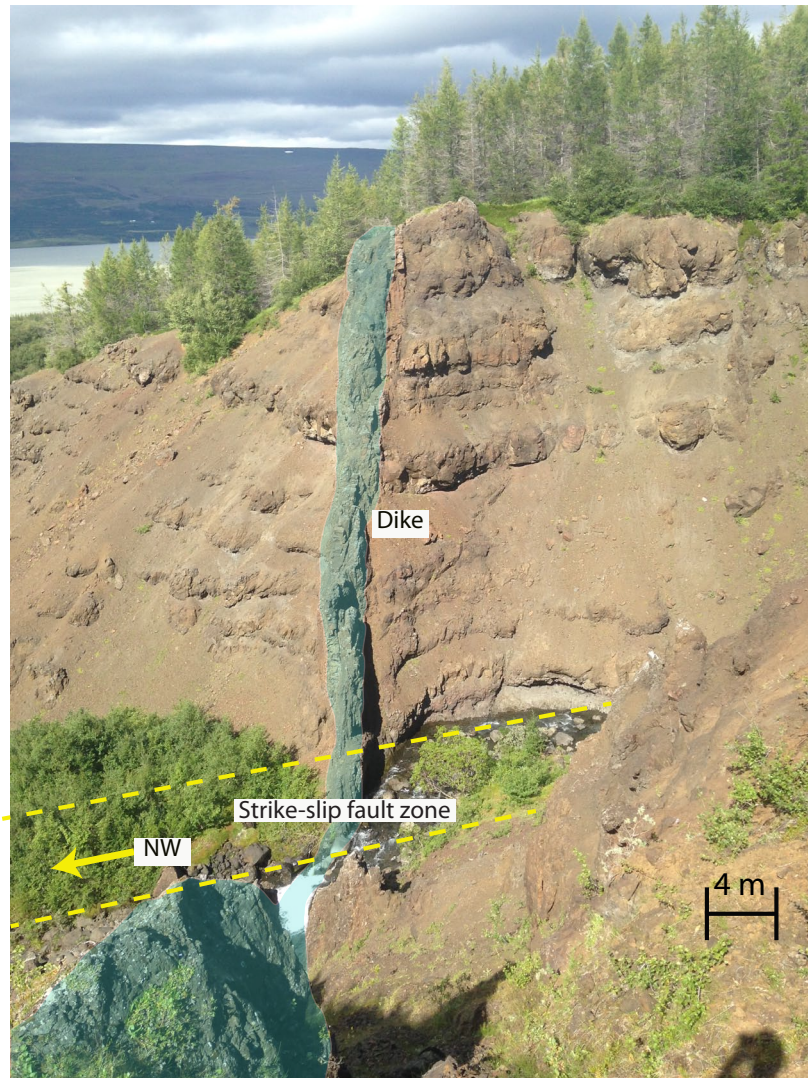


Figure 12. Photograph showing a NE-striking dike cutting a NW-striking strike-slip fault zone in the Hafursá river gorge. No horizontal offset is observed along the dike. Picture taken looking to the N.

4.1 Flexure Zone

Structures consistent with a flexure model are observed within the zone of higher dipping lavas (Figure 11). Small-scale conjugate normal faults with offsets of about 1 m as well as layer parallel slip are observed in some of the lavas found in this area (Figure 13). These are thought to accommodate the flexuring of the lavas in response to loading of the crust to the west. Another set of normal faults are found in the area, so faulting related to the flexure is inferred to be limited to conjugate normal faults with small displacements (1 m or less) that are found below the unconformity.



Figure 13. Deformation associated with the flexure zone. A) Small scale conjugate fault found along the lakeshore. Offset of ~ 0.5 m. Hammer for scale. B) Larger-scale conjugate offset (1 m) accommodating flexured lavas. Person in bottom right for scale C) Layer parallel slip is seen in flow top breccia. Red line denotes fault plane, which displays down-dip slickenlines. Hammer for scale.



4.2 Strike-Slip Faulting

Strike-slip faults are primarily oriented N-S to NNW-SSE with steep dips. They are typically found in stream cuts parallel to their strike. These faults are not as abundant as normal faults in the Lagarfljót valley. They are defined by planes that contain slickenlines with a plunge between 0° and 30° . In total there are 172 fault planes identified as strike-slip, with 94 of those also containing clear sense of shear (SOS) indicators (Figure 14). Of these, 19 are left-lateral and the remaining 75 are right-lateral. Strike-slip fault zones containing significant thicknesses of gouge were not readily identified in the field. For the 5 that were seen, gouge ranged from 0.5-1 m in width. Some fault planes display evidence of frictional melting, termed a “micromylonitic” structure, which is rare in mafic rocks (Passerini et al., 1997). This is a thin veneer that is comparable to mylonites proper and associated with high seismic-slip rates. SOS was identified by Riedel shears that are present and oblique to the fault surfaces (Figure 15). Offset markers are not observed across any of the fault zones, so displacement could not be quantified.

Cross-cutting relationships observed in the field indicate that a larger normal faulting episode post-dates the strike-slip movement. Fault planes displaying normal displacements cut strike-slip fault planes in multiple instances (Figure 15). Normal faults are also observed to cut strike-slip fault zones on a larger scale. Figure 22 shows the Hafursá River, which parallels a NW-SE strike-slip fault zone that is cut by NE-SW trending normal faults. This is seen along the

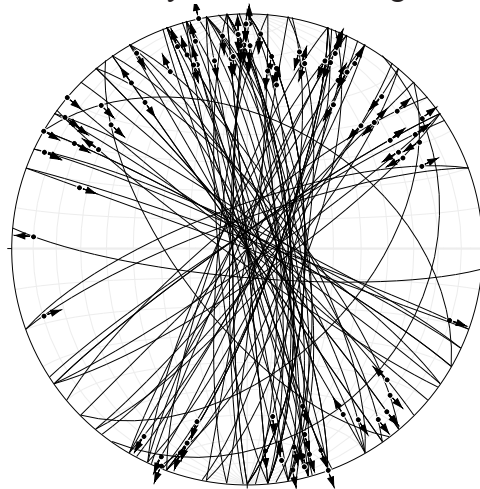


Figure 14. Stereonet showing strike-slip fault planes with a pitch of 0° - 30° and clear SOS indicators. Arrows show direction of slip. N = 94

A



Figure 15. Strike-slip features seen in the field. A) Normal fault plane cutting a strike-slip fault plane. B) Micromylonitic (glassy) features seen in the lower right above the pencil. These preserve horizontal slickensides in this picture. C) Right-lateral fault plane. Black dashed lines parallel slickenlines and yellow dotted lines indicate Riedel shears.

B



C



river Stadará 3 km to the south as well (Figure 11). In both cases a ~20 m waterfall marks the intersection of these two faults.

4.3 Dikes

Dikes are well exposed in the valley, with 182 identified and measured. Widths range from 0.3-10 m across, with most 2 m or less (Figure 16). The thicker dikes are typically found close together (Figure 17). Spacing of the dikes was on the order of 1-5 m with a parallel or en-echelon arrangement. The compositions are inferred to be tholeiitic based on thin section analysis, with phaneritic to porphyritic textures. Many dikes contain zeolites, typically calcium-rich stilbite, indicating some degree of alteration. Cross-cutting relationships in the field show multiple dike injections, which are common in and around rift segments. Strike of the dikes were either N-S or NE-SW with very few falling outside of this range (Figure 18). Excluding dikes that dip $>85^\circ$, eastward-dipping dikes outnumber westward-dipping dikes 68-29. This could be evidence of continued tilting of the lava pile after the dikes were intruded. The dikes display different cooling structures including columnar jointing and parallel fracturing. Faulting is indicated by fault gouge, Riedel shears and slickenlines that are found within the dikes and along dike margins. Of the 182 dikes identified, 69 of these contained fault gouge inside or on the margin of the dike (Figure 20). This indicates the normal faulting post-dates the dike intrusions. Width of the gouge ranges from a few centimeters to a meter wide in some places. Slickenlines are found along many of these faults, with SOS showing normal faulting is most common.

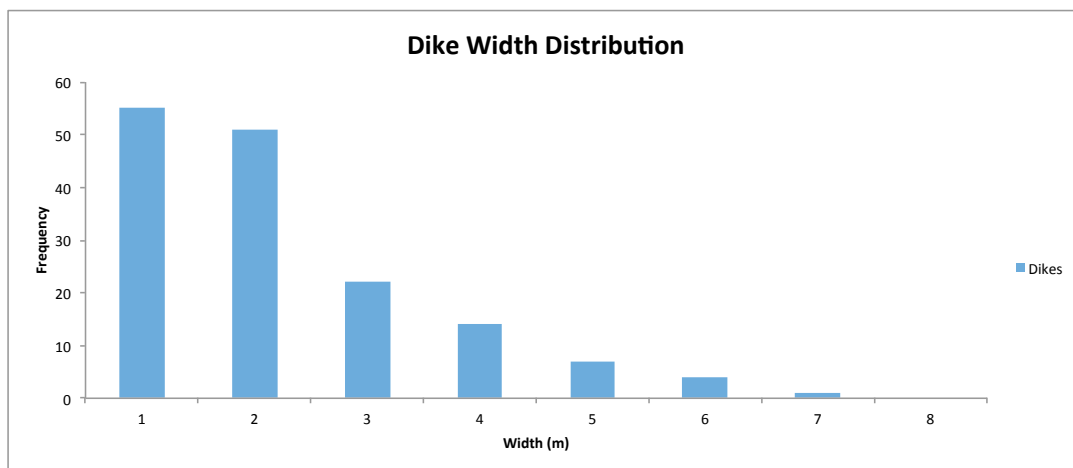


Figure 16. Histogram of dike widths.

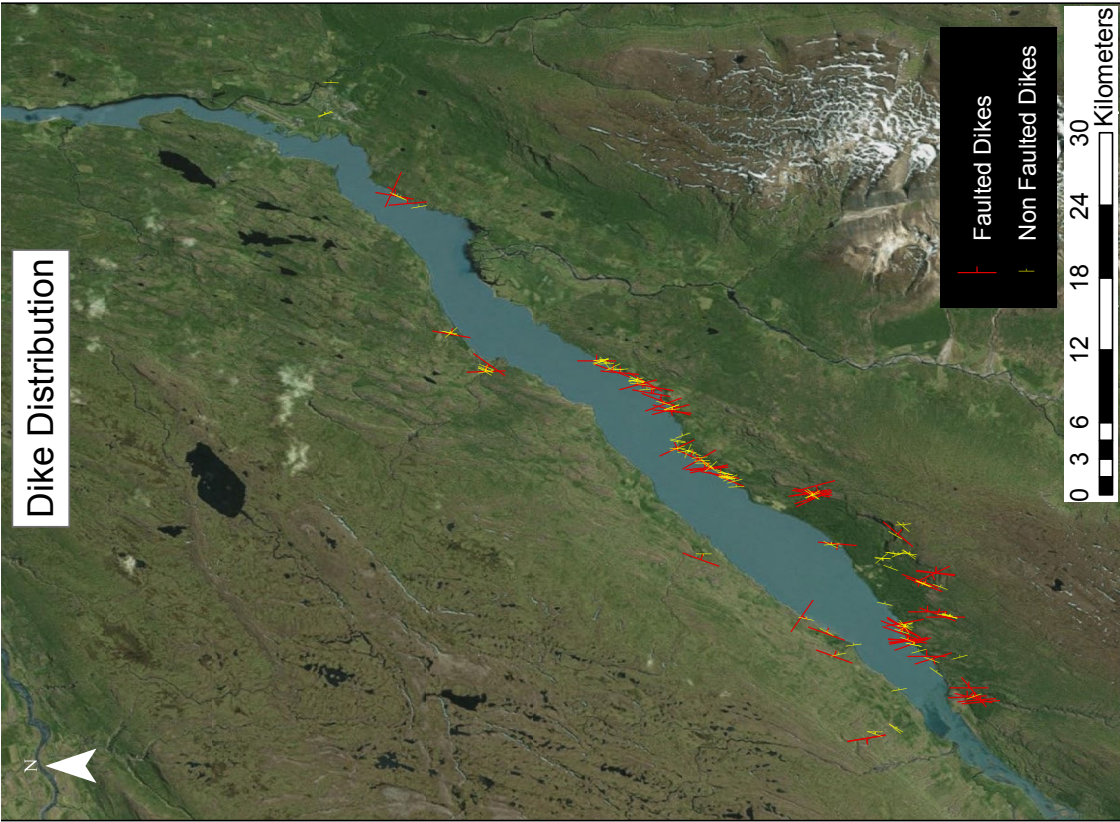
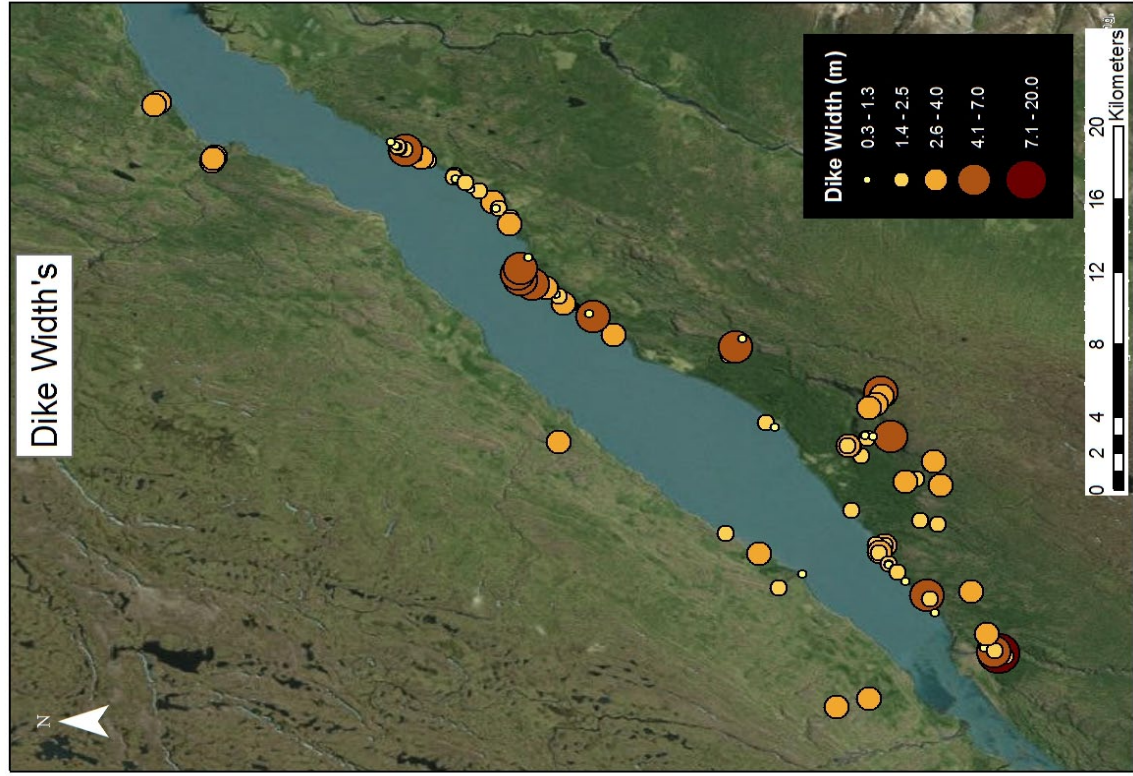


Figure 17. Map on left displaying orientations of dikes. Yellow are undeformed and red are faulted or have fault gouge on their margins. Map on right shows how thickness of the dikes varies spatially. Darker colors indicate thicker dike intrusions.

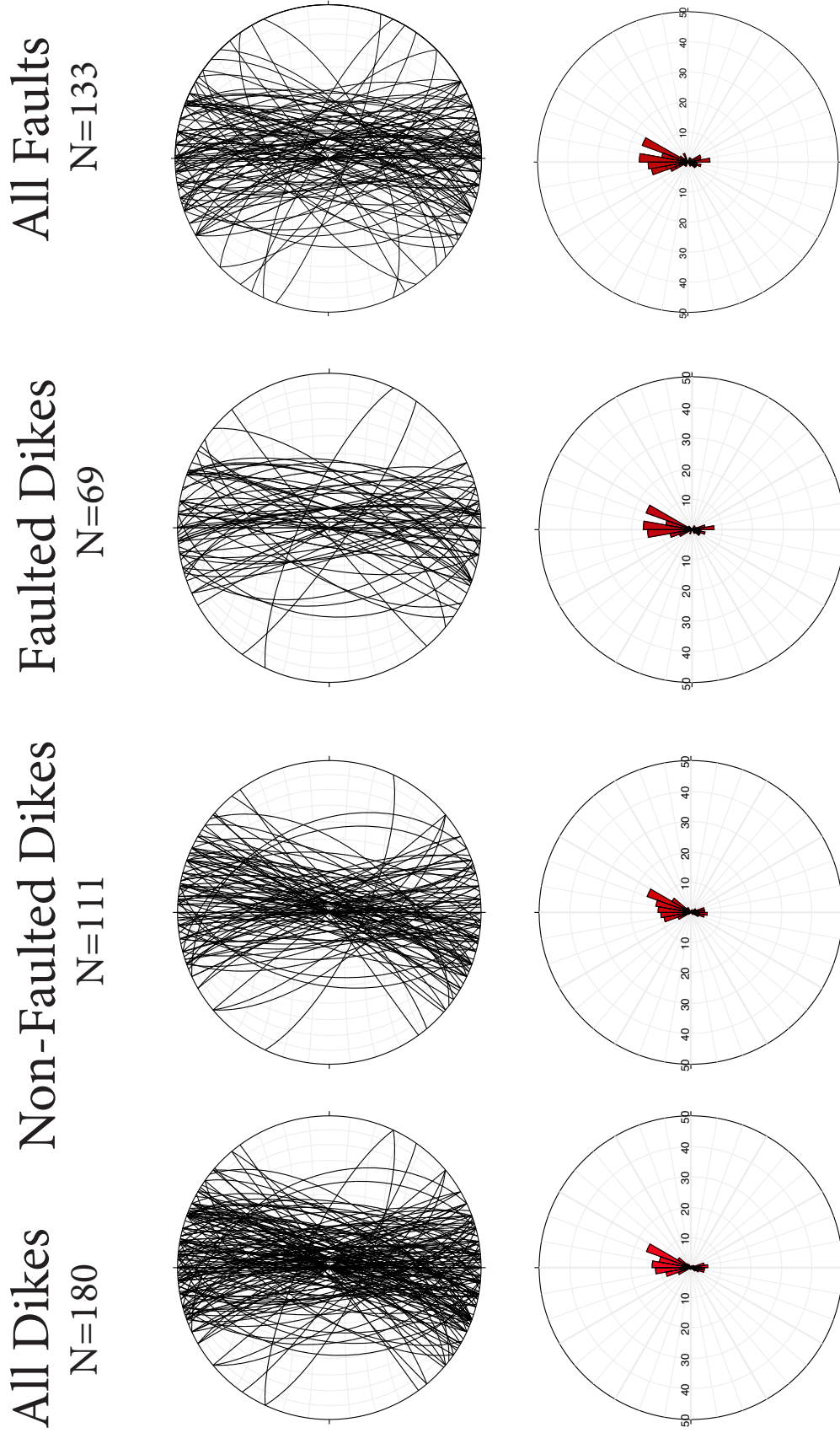


Figure 18. Stereonets and rose plots showing orientations of dikes and faults within the study area. Rose plots are constructed based on the right-hand-rule. A strong N-S and NE-SW orientation is seen in the faults as well as in the dikes.

4.4 Normal Faulting

Normal faulting in the region is the dominant mode of faulting and the most recent. As previously explained, small-scale normal faults are seen to accommodate flexure of the lavas. Larger scale and more recent normal faults are concentrated along dike margins, but are not uncommon in other areas. In contrast to the strike-slip faulting, most of the normal faults define clear fault zones with SOS indicators and fault gouge. In total 116 vertical faults and fault planes were identified, with 57 of these having clear SOS indicators (Figure 19). The faults have a strike of NNE-SSW and are dipping 70° on average. Slickensides are common on these fault surfaces, and in some cases a “micromylonitic” structure is observed (Figure 20). The best preserved slickenlines are seen in syn-kinematic mineral growth on the fault surfaces, primarily quartz and calcite. The fault zones are most commonly ~ 1 m wide, but ranged from 0.2 to 10 m across the study area. Cumulative gouge thickness from all measured faults is on the order of 100 m. The largest observed vertical separation along a single fault was 8 m, but based on the width of some of the fault zones such as the one seen in Klifa, the total offset is likely much higher (Figure 21). It should be noted that although there are more strike-slip faults recorded than normal faults, the data are likely skewed towards these structures based on the objective of the study to study rift-parallel strike-slip faults.

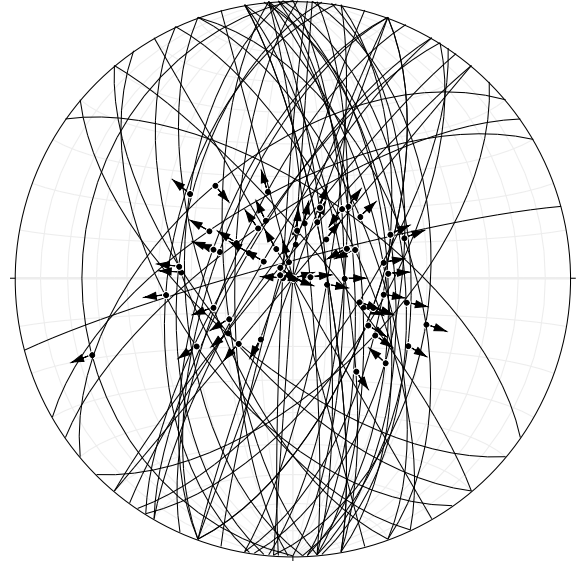


Figure 19. Stereonet showing normal fault planes dipping between 60° and 90° with clear SOS indicators. Arrows indicate slip direction. N = 59

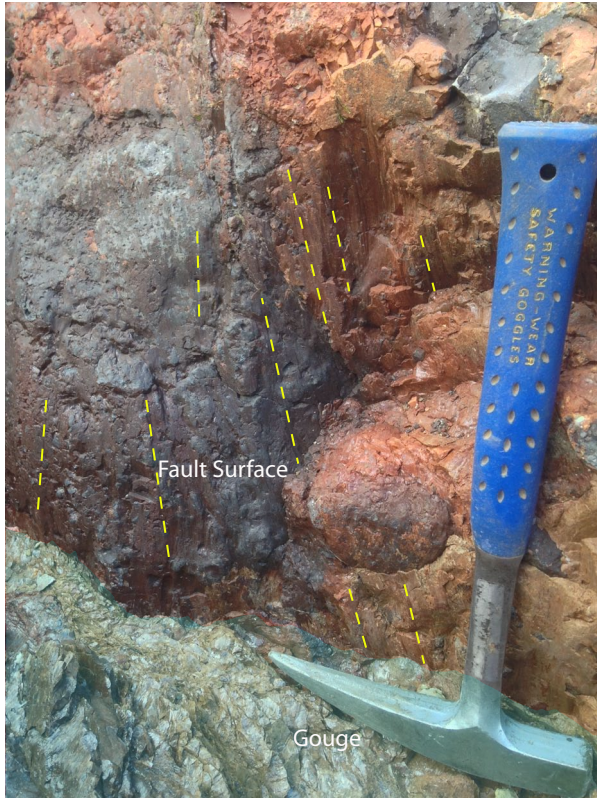


Figure 20. A) Normal fault surface showing a polished slickensided surface with down-dip slickenlines (yellow dashed lines). Fault gouge is adjacent to the fault plane and a micromylonitic structure was observed on the fault plane. B) Dike (on right) with adjacent fault gouge displaying normal kinematics. Hammer in center for scale. C) Faulted dike margin with Riedel shears (yellow dashed lines) offsetting material in the gouge in a normal sense.



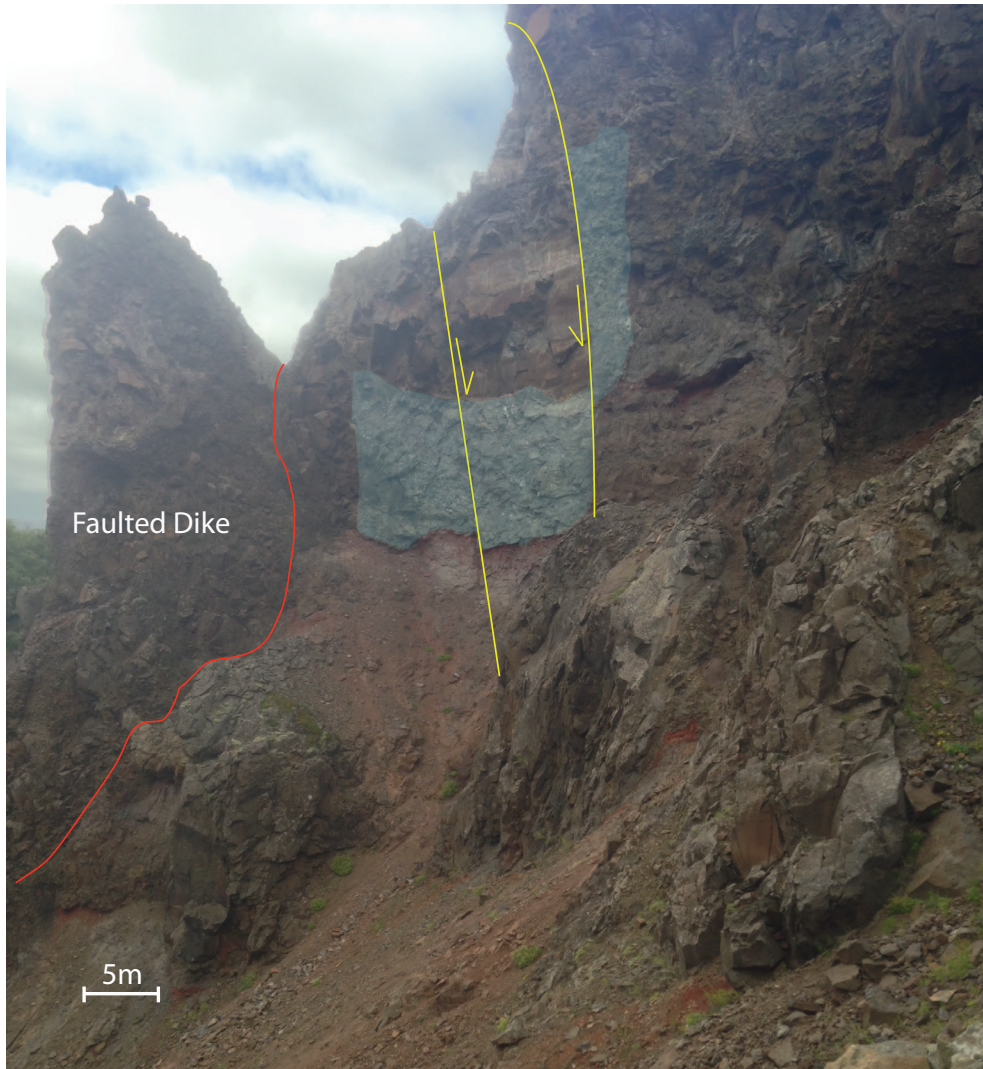


Figure 21. Large normal fault zone found in the Klifá river. Vertical separation of approximately 10 m is observed on one of the normal faults (yellow line on right). Red line denotes contact of dike (left) and lava units. This area contains multiple large normal faults and massive damage zones 10's of meters wide.

4.5 Hafursá River Fault Zone

The Hafursá River preserves a zone of faulting that exemplifies the overall deformation in the study area. The river is parallel to a N-S striking segment of a right-lateral normal fault which bends around to a NW-SE orientation at the contact of a large normal fault (Figure 22). NNE-SSW-striking dikes cut the gently dipping lavas and the strike-slip faulting, and are typically 1-5 m in width. Cross-cutting relationships show that more than one dike injection event occurred. Normal faults mostly occur along dike margins. Some cut the lava's with up to 8 m of vertical separation seen on a single fault. Kinematic indicators in the damage zone are clear and well preserved with abundant Riedel shears, slickenlines, and vertical separation. Down-dip slickenlines are found primarily along dike faces. Horizontal slickenlines with right-lateral Riedel shears are seen along the length of the river, with larger 1x1 meter fault surfaces near the NW bend in the river. Multiple instances of normal fault planes cutting a strike-slip fault plane occur along the length of the stream. Displacement and magnitude of the strike-slip faulting were not determined as no markers are seen to be offset and no gouge is found adjacent to the strike-slip fault planes. The normal faults have much clearer kinematics, with a cumulative offset of >20 m and gouge width totaling >10 m over a 2 km transect.

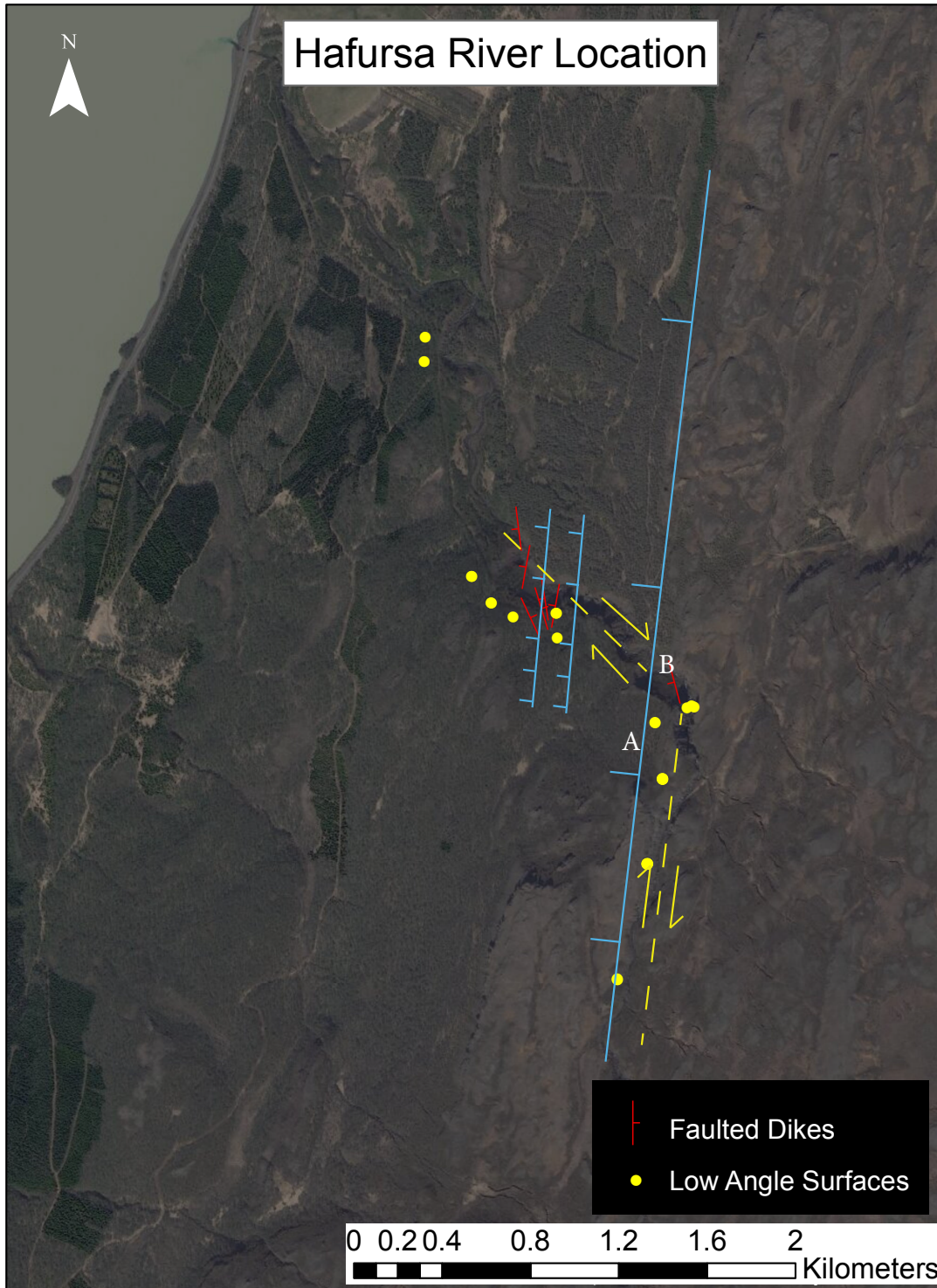
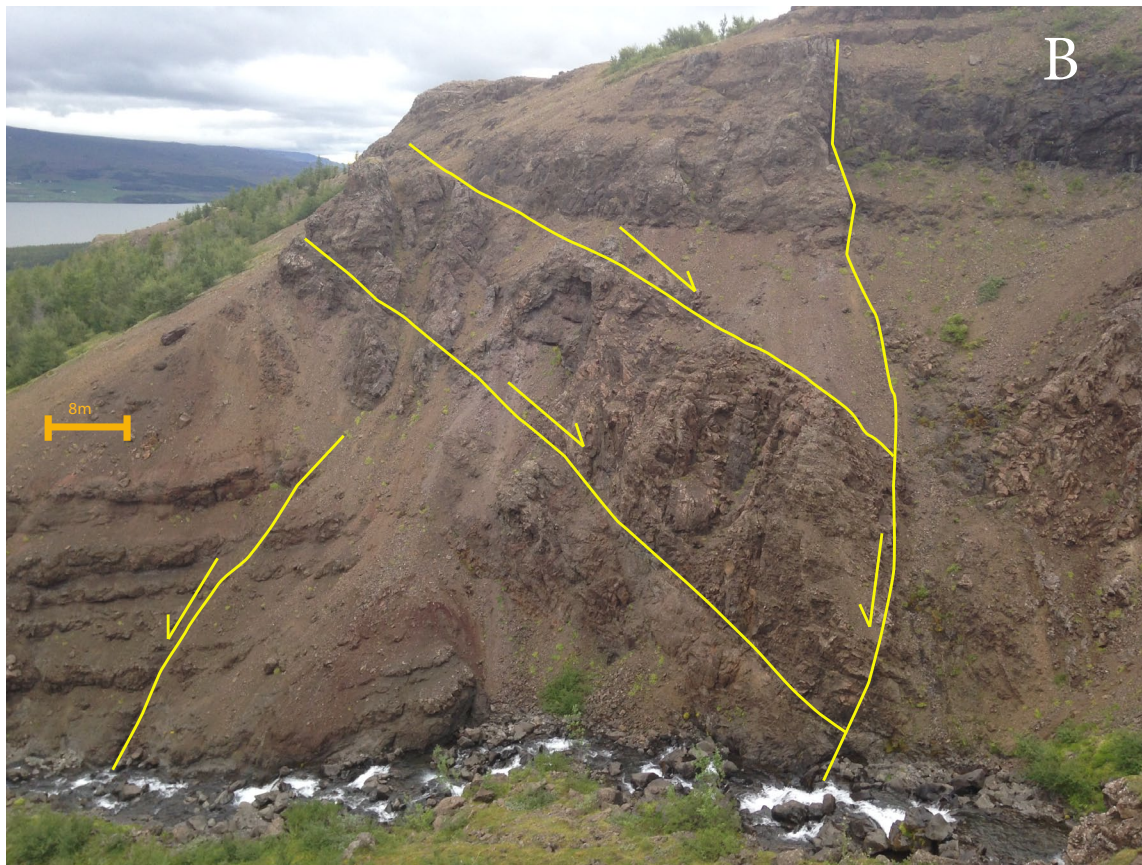


Figure 22. Hafursá River location, with interpreted structures. NNE-SSW normal faults (blue) cut a N-S strike-slip fault zone that bends to a NW-SE strike at the contact of a large normal fault zone (A). This zone contains a series of synthetic and antithetic normal faults (yellow) that are outlined in the figure below (B).



5. Interpretation

The following table outlines the main interpreted tectonic and volcanic events of the Lagarfljót Valley (Table 1). This information is a combination of previously compiled studies and more recent observations.

Event Order (youngest- oldest)	Event	Structures & Orientations	Notes
0 Ma	Westward subsidence due to loading along the NVZ?	Tilted lavas along N-S axis	High angle reverse fault indicators, dominant eastward dip of dikes
	NW-SE extension	NNE-SSW normal faults cutting everything and found mostly along dike margins.	High-angle slickenlines, offset beds, cross-cutting dikes and strike-slip faults
~5 Ma	NW-SE extension	NNE-SSW dikes injected perpendicular to spreading direction ~4.4 Ma	Age date from Garcia (2004)
	N-S to NNW-SSE trending	N-S right-lateral strike-slip faults develop	Low-angle slickenlines and Riedel shears in outcrop, focal mechanisms. Crosscut by dikes and normal faults

	In-filling of rift valley during period of reduced volcanism?	N-S sedimentary unconformity with moderate dip (9°) overlays flexure zone with undeformed and gently dipping lavas capping it	East Iceland regional observations Saemundsson, 1974
~8 Ma	Ridge jump from west to east? Decreased volcanism	Lagarfljót flexure zone is formed along N-S axis, with lavas dipping up to 25° to the west	Small-scale conjugate normal faulting and layer-parallel slip Watkins & Walker, 1977, Walker, 1974, Saemundsson, 1974
	E-W extension and volcanism associated with Thingmuli central volcano	N-S dikes injected into lava pile ~8.8 Ma	Walker, 1974, Garcia, 2004
10 Ma	Flood basalt's erupted from Thingmuli and surrounding volcanoes	Lava pile constructed 7-9 Ma	(Oskarsson, 2014), (McDougall, 1976), (Moorbath et al., 1968)

Table 1. Inferred geologic events of the Lagarfljót Lake study region through time.

In general the Lagarfljót Valley is characterized by NNE-SSW striking normal faults cutting N-S right-lateral strike-slip fault zones. NE-SE-striking dikes also cut the strike-slip fault zones. Of these, 40% are faulted along the dike margins or within the dike itself. Aerial photography show a strong NE-SW preferred orientation of lineaments, which parallel the trend of the lake itself. N-S lineations are also present, though not the preferred orientation in the study area. Local orientations of structures however are much more varied, with significant numbers of N-S dikes and fault planes. A NW-SE component of faulting is also observed, mostly prevalent in the Hafursá river fault zone (Figure 22).

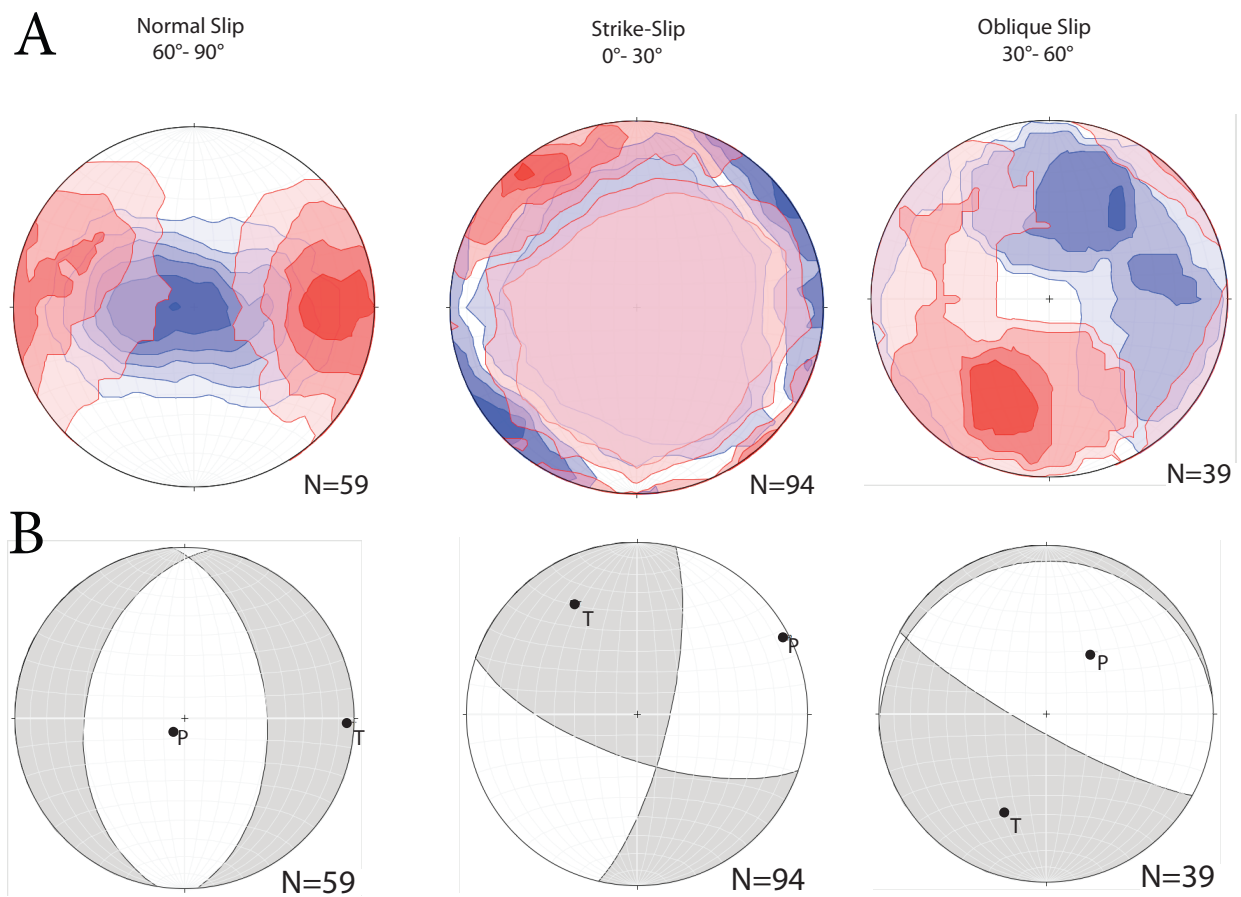


Figure 23. A) Contoured P (blue) and T (red) axes using the Kamb contouring method (Kamb, 1959). B) Focal mechanism diagrams showing nodal planes based on statistically defined maximum of P and T axes. See text for values.

Kinematics point to normal faulting as the primary mode of deformation postdating dike intrusion, with the average fault plane striking 010° and dipping 40° to the west (Figure 23). The strike parallels the overall NNE trend of dikes and normal faults in the study region. The strike-slip faults strike mostly N-S or NNW-SSE. Kinematics show the typical fault plane among the strike-slip faults is striking 012° and dipping 74° to the east, with an overall dextral sense of motion (Figure 23). The typical oblique slip fault planes are striking at 120° and dipping 80° to the south west.

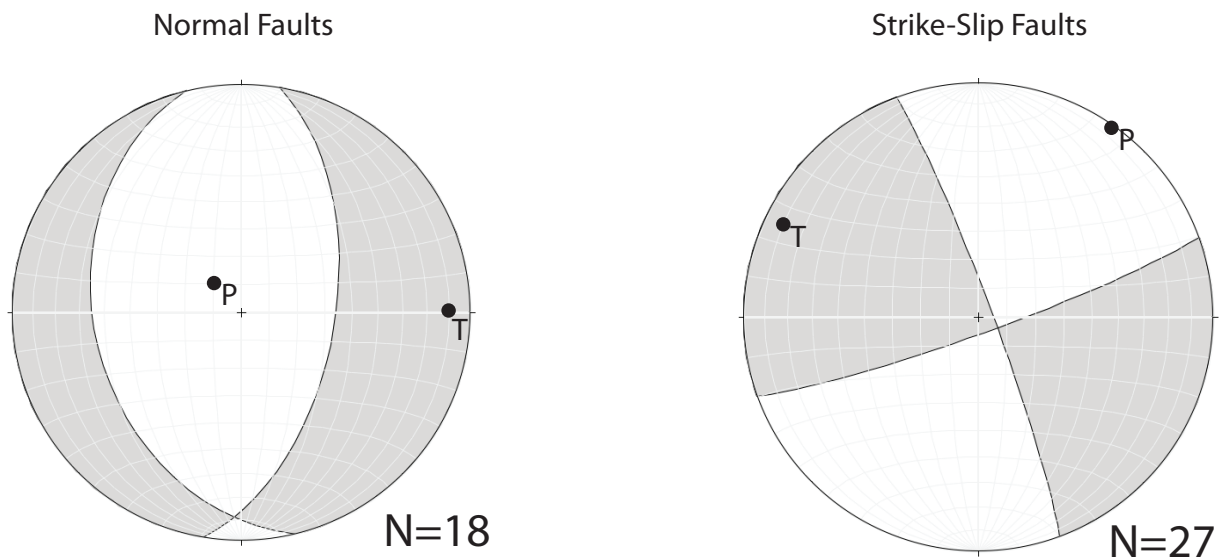


Figure 24. Focal mechanisms produced from Hafursá fault zone. Typical normal faults are NNE striking and dipping steeply to the east. Strike-slip fault shows NW-SE orientation and right-lateral movement.

The kinematic results from Hafursá are in line with the larger scale orientations of faulting. In the field, NE striking normal faults cut older N-S to NNW-SSE-strike-slip fault zones. The kinematics mostly agree with observations in the field of a NNW-SSE high angle right-lateral strike-slip fault being cut by a series of N-S westward-dipping normal faults (Figure 24). The Hafursá fault zone strikes more NW than the regional orientation, but overall the kinematics and the field observations agree.

5.1 Estimates of net displacement from gouge thickness

A roughly linear relationship has been established between fault gouge thickness and fault slip on a log-log plot (Almendinger et al., 1989, Scholz, 1987). The relationship is approximately $70 \cdot T = D$ where T is gouge thickness and D is displacement. This can be used to conservatively estimate average displacements along normal faults in the study area, assuming displacement occurred all at once and not as a result of multiple events. This also does not account for the distinction between gouge, breccia, and cataclasite that can be made in the field, but for this purpose are grouped together. Estimates of net displacement on strike-slip faults are not made due to the lack of fault gouge and offset markers. Forslund & Gudmundsson (1992) carried out a study of normal faults in Iceland, with one of the components looking at the D/T ratio. They showed that the ratio in Iceland is approximately 22, or one-third of the ratio determined by previous work. Scholz (1987) explains that breccia thickness should be inversely proportional to the hardness of the rock. Thus this lower ratio is likely due to the softer basalt lithologies compared to quartzo feldspathic rocks used in previous studies (Forslund & Gudmundsson, 1992).

Average gouge thickness among normal faults in the Lagarfljót area is ~1.3 m, which gives an estimate of 10's of meters of displacement along individual faults. The total gouge thickness among measured faults is 75 m. This corresponds to total displacement values in the 1000's of meters along these normal faults (Figure 25).

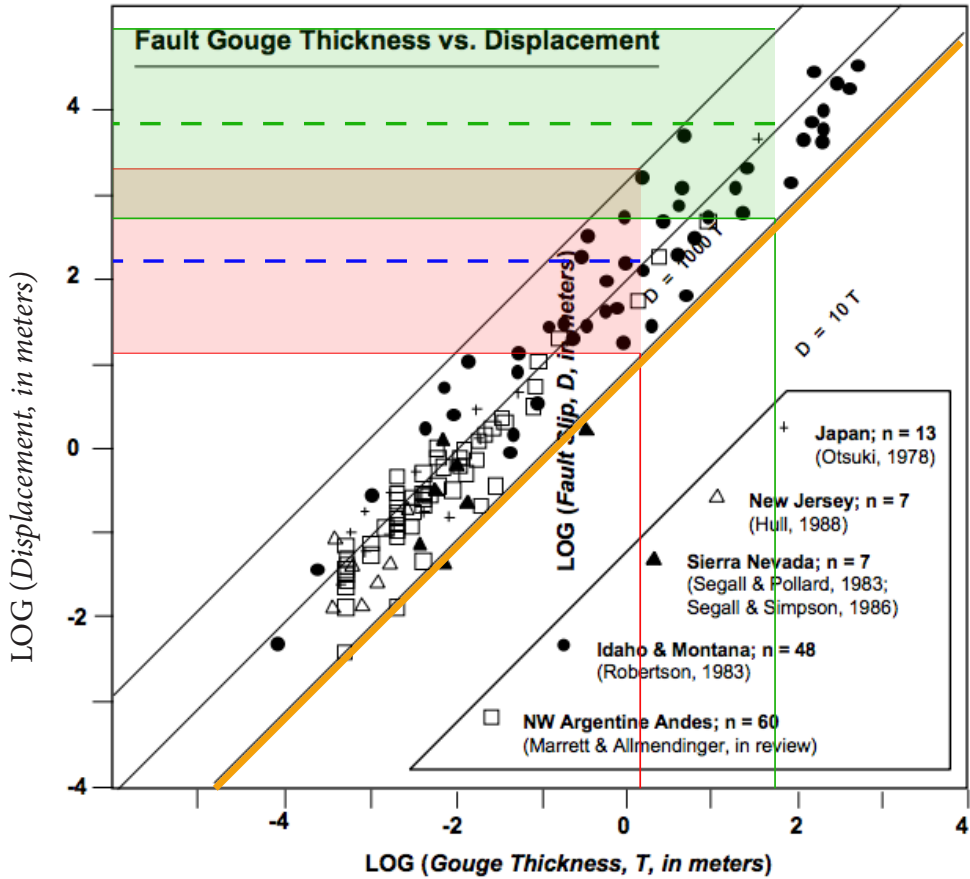


Figure 25. Log-log plot of fault gouge thickness vs. fault displacement from Allmendinger et al. (1989). The red box illustrates the range in displacement values along an average fault within the study area. The green box illustrates the range in values for total displacement among all faults studied. Work by Forsund & Gudmundsson (1992) suggests that the lower limits should be used due to rheologically weaker rocks in Iceland than those used in the study that lead to the figure above (orange line). (Modified from Allmendinger et al. 1989).

6. Discussion

An investigation of the Lagarfljót area reveals it is a zone that has been subjected to multiple episodes of deformation, and can provide clues towards larger questions that are currently being debated relating to regional tectonic processes. It is widely accepted that the locus of spreading has jumped east in the past as the American-Eurasian plate boundary drifts west relative to the Icelandic hotspot. The hotspot can be considered fixed on these time scales (Saemundsson, 1974; Helgason, 1984; Martin et al., 2011; Garcia et al., 2003). However, the number and timing of these events is still largely unknown, in part because of a paucity of reliable dates of dikes and lavas in many regions of Iceland. Thus, the structural and kinematic data can offer clues to help in determining paleo-rift processes.

6.1 Origin of dikes and normal faults

Dike orientations are good indicators of ancient spreading directions, assuming there has been no tilting or vertical axis rotations of the dikes. The presence of a N-S and a NNE-SSW set of dikes in this study points to a probable change in the local spreading direction at some point in time. Looking at the limited age dating done in this area, Garcia et al. (2004) published two age dates using the K-Ar whole rock dating method. These conveniently are from a N-S striking dike east of the unconformity and a NNE-SSW dike that is just to the west of the unconformity. The N-S dike produces an age of 8.8 ± 0.2 Ma., while the NNE-SSW dike produces an age of 4.6 ± 0.1 Ma. Previous mapping of dikes in this region by Walker (1974) show a strong N-S orientation, and are attributed to the Thingmuli fissure swarm (Carmichael, 1964). Mapping of the geology just to the south, in and around Múli, was carried out by Gudmundsson (1978). These results agree with data from Lagarfljót, showing the same two populations of N-S and NNE-SSW dike orientations. Present day strikes of structures found in the closest fissure swarm Kverkfjöll mostly fall in the range of 015° - 030° (Hjartardottir & Einarsson, 2011). It is hypothesized that the N-S set of dikes are related to the Thingmuli volcanic complex (Figures 6, 26). This complex is thought to be part of a flank zone to the east of a N-S oriented spreading center that was active 8-12 Ma (Moorbath et al., 1968; Martin et al., 2011; Oskarsson

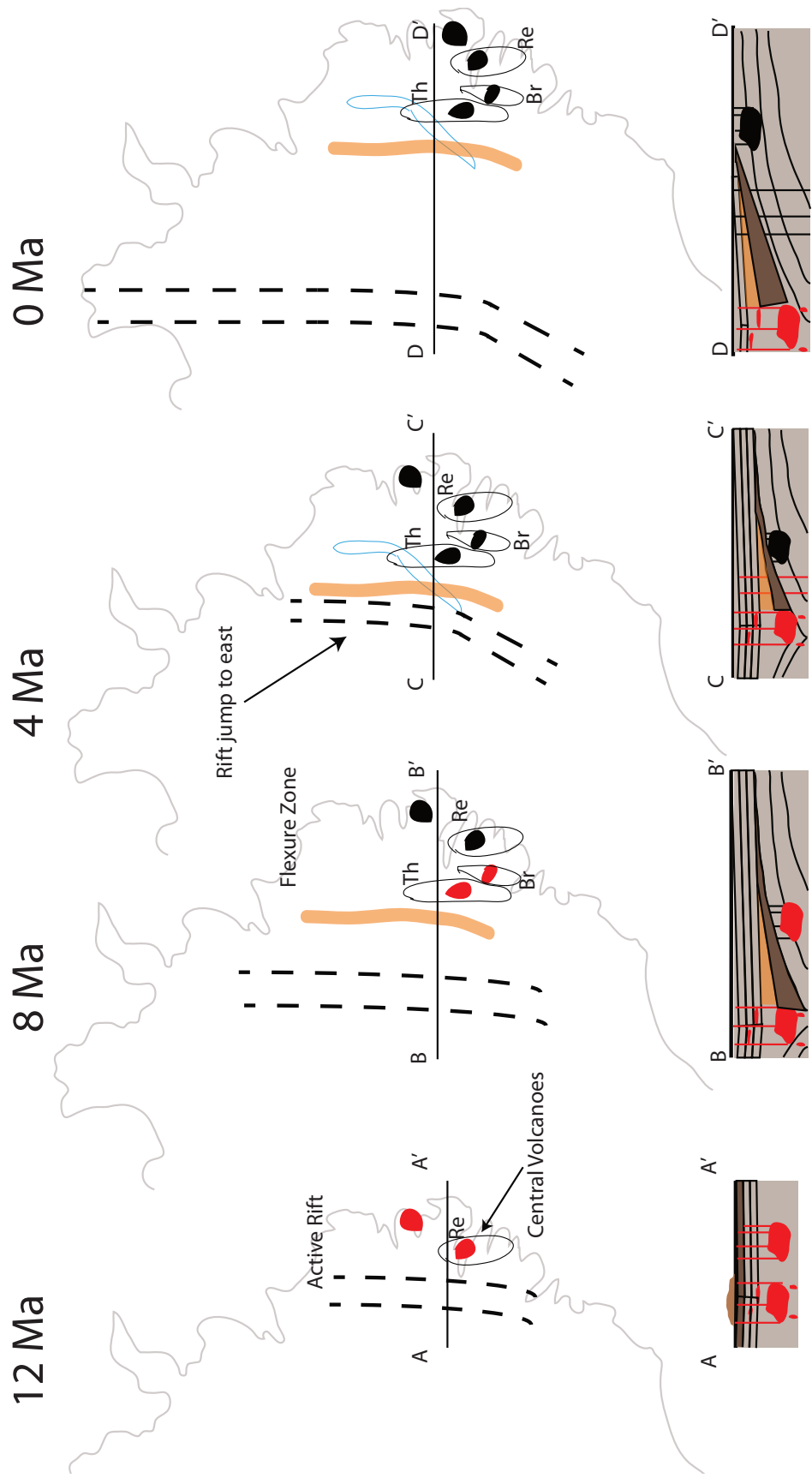


Figure 26. Model for the development of the Lagarfljót region based on age dates, dike orientations, and previous models (Martin et al., 2011; Garcia et al., 2004; Moorbath et al., 1968). Red color indicates active volcanism while black indicates inactive volcanism. 12 Ma, initial development of the Reyðafjörður Volcanic zone as a flank volcano to a newly initiated rift zone in the east. 12-8 Ma, as spreading continues flank volcanism is transferred from Reyðafjörður to the Thingmuli and Breidaluder systems with associated N-S fissure swarms at ~10.5 Ma (Helgason, 1984). These systems are eventually moved far enough off axis that volcanism ceases. A flexure zone (brown) developed in response to rifting, and was in-filled with sediments during a period of decreased volcanism. 8-4 Ma, another rift jump to the east (~6-4) Ma brings the rift into the southern vicinity of present day Lake Lagarfljót. NE dikes and normal faults associated with the adjacent spreading center form. 0-4 Ma, the region is transported away from the axis as spreading continues at a steady rate of 20 km/my.

& Riishuus, 2014). A relative quiescence of volcanism is thought to then have taken place from 8-4 Ma, along with a series of ridge jumps (Helgason, 1984; Martin et al., 2011). This is likely when the Lagarfljót flexure zone and overlying sedimentary package were formed, as a response to rifting in a magmatically starved system (Figure 27) (Saemundsson, 1974).

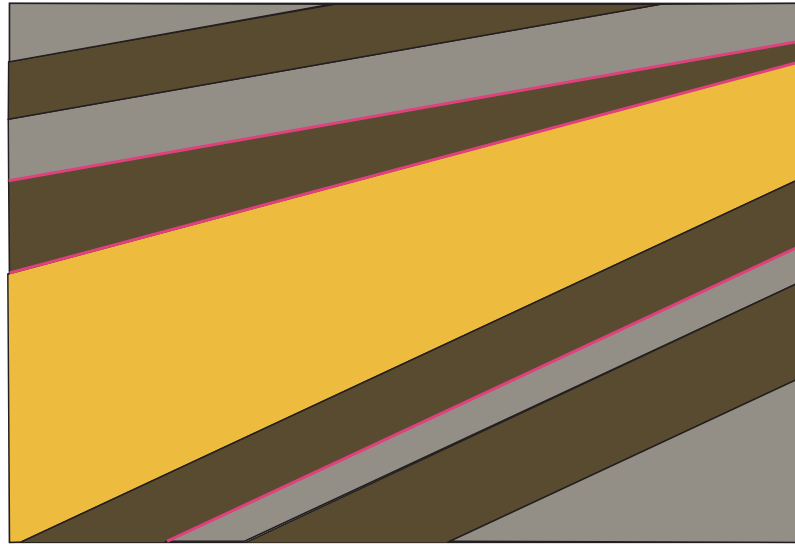


Figure 27. Cross-sectional view showing basaltic flows dipping at 25° overlain by a sedimentary package and capped by another gently dipping basaltic lava sequence. Red lines indicate contacts between successive layers of lava where sediments have been cooked by a subsequent flow.

During this time, the direction of extension in this region could also have rotated from E-W to a more NW-SE direction, consistent with the spreading direction seen today. The Lagarfljót region at 4 Ma was likely close to the active spreading center, so dikes forming there would propagate to this area and be emplaced in a NNE-SSW orientation. This model would be consistent with age determinations and previous models proposed for ridge jumps of the NVZ (Martin et al., 2011).

As is the case in most volcanic terranes, dike injections and normal faulting are inherently related. Dikes at depth initiate faulting at the surface which propagate downwards (Rubin & Pollard, 1988). The faults commonly nucleate as fissures at the surface and grow vertically as displacement continues (Grant & Kattenhorn, 2004). Dikes can also serve as zones of weakness where slip occurs, with 40% of the dikes examined showing some degree of faulting. However this does not indicate the actual cause of the faulting, or control of faults on dike margins. The dikes and normal faults are accommodating extension related to rifting. Using a simple trigonometric relationship where β = the average dip of the faults and h = the cumulative slip of the faults, the total extension (a) accommodated in this area can be estimated (Figure 28). This

can be done using values previously determined for the area:

$$\cos(80^\circ) = a/1000$$

$$a = 173 \text{ m}$$

This gives a lower limit on the amount of cumulative throw seen in the valley over a roughly 8 km wide area. Dividing the throw by the width of the area gives an estimate of percent extension:

$$(170/8000) * 100 = \sim 2\%$$

Thus the Lagarfljót Valley has undergone a minimum of $\sim 2\%$ extension related to faulting. This agrees with previous findings in the region, where percent extension due to faulting ranges from 0.6% to 5.3% (Gudmundsson, 1984; Forslund & Gudmundsson, 1992).

6.2 Origin of strike-slip faulting

Dikes and associated normal faults are common occurrences throughout Iceland and at all rift zones. Strike-slip faults are also commonly found in Iceland, mostly concentrated in the transform zones (SISZ, TFZ) and oblique spreading segments like the Reykjanes Ridge (Morgan & Kleinrock, 1991; Gudmundsson, 1996; Einarsson, 2008). However, the presence of N-S right-lateral strike-slip faults that are parallel to the spreading axis are not widely described, and deserve some deeper consideration in the context of tectonic models for ridge development processes. These faults are cutting the lavas and are cut by the NE dikes and normal faults. Assuming the NE dikes are all $\sim 4\text{-}5$ Ma in age and the lavas are 8-10 Ma, the strike-slip faults could have formed at any time over a ~ 5 million year period. We will investigate possible scenarios of formation for this population of faults, and determine the likelihood for each.

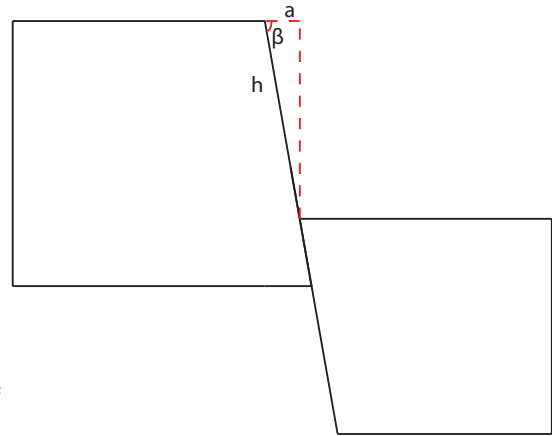


Figure 28. Schematic showing how throw can be estimated for one fault. Cumulative throw is estimated from cumulative displacement. a = total extension, β = average dip of faults, h = cumulative slip.

6.2.1 Bookshelf faulting between adjacent fissure swarms

A recent study by Green et al. (2013) found bookshelf faulting accommodating motion between the Askja and Kverkfjöll fissure swarms of the NVZ (Figure 29). As spreading is transferred westward from the Kverkfjöll fissure swarm to the Askja fissure swarm, a deforming relay zone has been interpreted from analyzing nodal planes in the seismic data.

A left step in the ridge leads to an overall right-lateral shear zone, which is accommodated by NE-SW (ridge

parallel) left-lateral bookshelf style faults (Figure 29). It is inferred that these bookshelf faults formed along pre-existing weaknesses in the crust oriented $\sim 020^\circ$ and have since been rotated clockwise to 040° as slip occurs. The calculated slip rate is 0.9-1.8 km/Ma along each fault. This type of block rotation in overlapping spreading segments has also been observed along other spreading environments (Abbate et al., 1995; Mulunch et al., 2013).

However putting this analysis of transform motion between fissure swarms into the context of the Lagarfljót study area, issues arise. In Lagarfljót the scale of the faults is much smaller, and the setting is also different. The closest central volcano is Snaefell, which is observed to have a very small associated fissure swarm, ~ 2 km long, and is also associated with much more recent activity than Thingmuli (Hards et al., 2000). Even if there was an overlapping fissure swarm to the west, it would require left-lateral bookshelf faults to accommodate a left step in the spreading segments. The faults observed in this study have right-lateral kinematics.

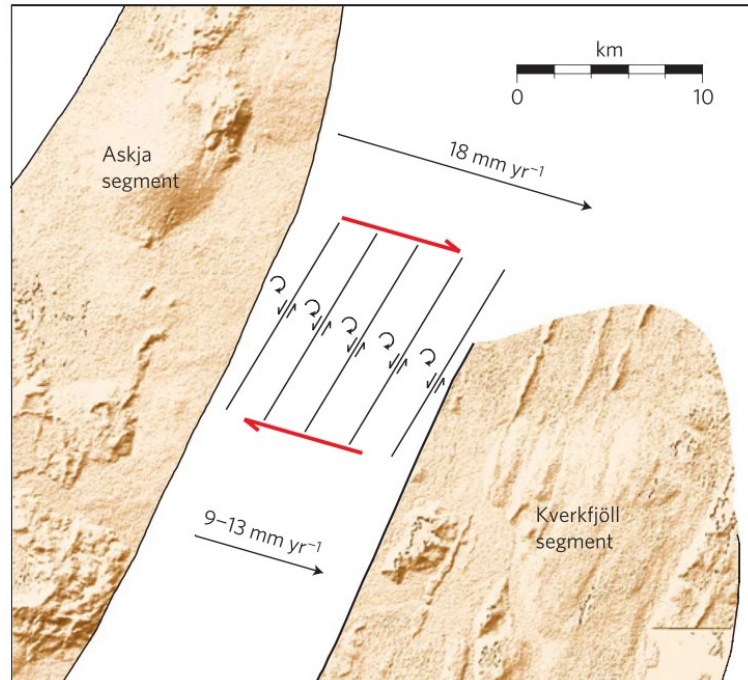


Figure 29. Schematic for strike-slip faulting seen in NVZ that has been proposed by Green et al. (2014). A left step in these overlapping segments creates a right-lateral shear zone that is accommodated by block rotation along left-lateral bookshelf faults.

Thus, though we see this type of faulting in the NVZ today, it is unlikely to be the mechanism that led to the formation of the strike-slip faults around Lagarfljót.

6.2.2 Abandoned Transform Zone

The mechanics of rift propagation give rise to abandoned transform zones, which are arguably observed in the TFZ today (Figure 1). As a rift propagates, it leaves in its wake a series of old transform zones (Morgan & Kleinrock, 1991). In Icelandic crust, these transform zones are typically defined by bookshelf faults that are orthogonal to the overall shear direction. If the strike-slip faults observed in the Lagarfljót area are bookshelf faults related to an abandoned transform, they would be part of an overall left-lateral shear zone accommodating a right step in the ridge (Figure 30). A right step would require a N-S oriented

spreading center observed in northeast Iceland. At present, there is no evidence to suggest the northern ridge segment was located to the east. There would also be some type of evidence of a roughly E-W oriented transform zone in the form of a lineament or series of lineaments in the region. Though there are multiple volcanic complexes to the east, they have been dated to >12 Ma in age, with no (unconformable) younger lavas overlaying them (Helgason, 1984). With many of the telltale signs of a spreading axis missing, it is reasonable to say there is no spreading segment to the NE of Lagarfljót that would have been active at the time of the strike-slip fault formation. Thus it can be concluded that the strike-slip faulting here is unrelated to a transform zone found between overlapping segments of a MOR.

6.2.3 Strain partitioning from oblique plate movement

Strain partitioning has been studied in various regions of Iceland, most notably in the Reykjanes Peninsula where the ridge is oriented $\sim 30^\circ$ from the absolute plate motion (Clifton & Kattenhorn, 2006). It has been proposed that 70% of all spreading segments in the world

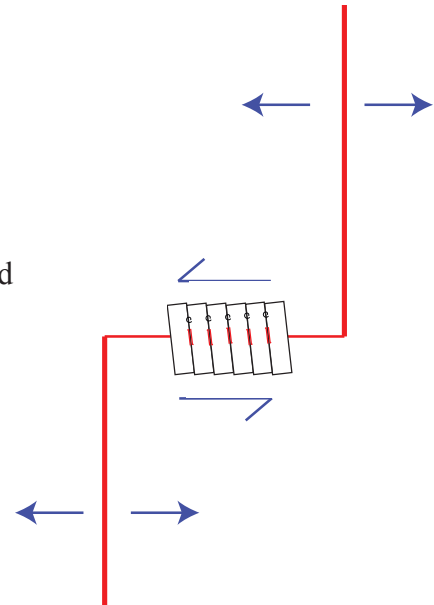


Figure 30. Schematic showing how a right step in the spreading axis would lead to a left-lateral shear zone accommodated by N-S right-lateral strike-slip faults.

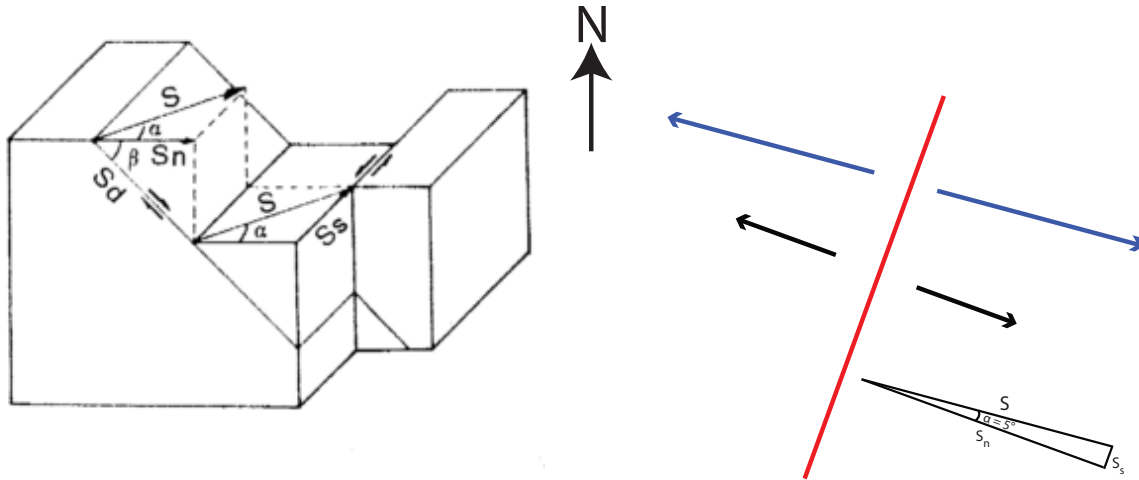


Figure 31. A) 3D model from Passerini et al. (1997) showing strain partitioning at an oblique rift. Variables are as follows: α = angle between spreading and extension directions, β = angle of dip of normal faults, S = spreading direction, S_d = displacement along normal fault, S_n = normal fault component of spreading, S_s = strike-slip component of spreading. B) 2D map view of this model applied to this study area. Blue arrows are spreading direction of 105° and black are extension direction of 110° . Triangle shows S_n to S_s relationship in this example. Shear in this case would be left-lateral. If the spreading direction was 115° the triangle would be the same but give rise to right-lateral strike-slip faults.

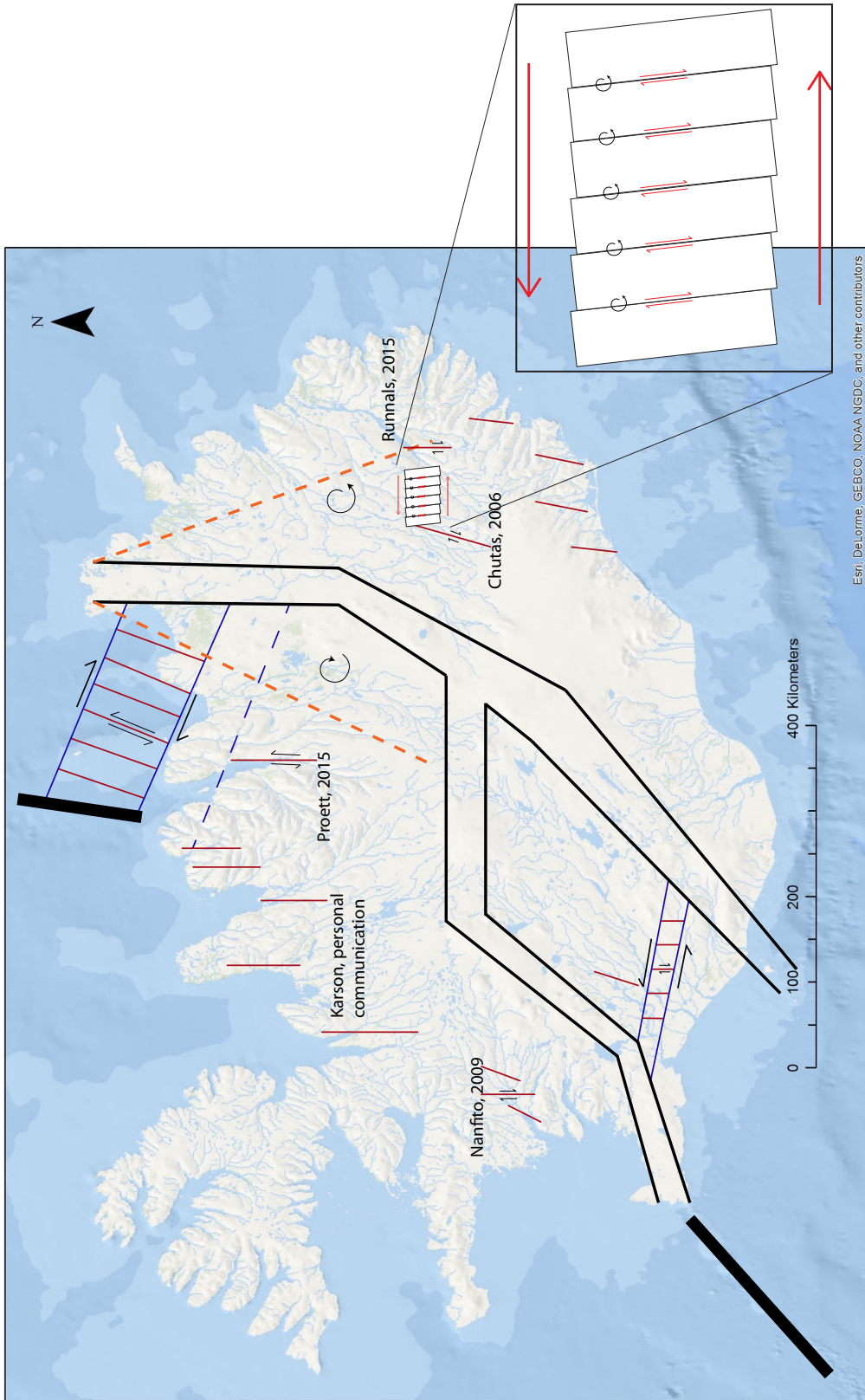
have some degree of obliquity to the direction of absolute plate motion (Woodcock, 1987). In an obliquely diverging segment of a spreading center, a component of rift-parallel shearing (strike-slip faults) is observed. Passerini et al. (1997) suggest that such a mechanism could be responsible for the formation of ridge-parallel strike-slip faults observed in southern Iceland. They derive an equation based on simple kinematics that determines the ratio of strike-slip to normal throw (SS/N). This is based on dip of the normal faults (β) and the angle between absolute plate motion and the direction of extension (α). Assuming a constant dip of the normal faults, the ratio increases as the obliquity angle increases. Using an average NE dike orientation of 20° , a reasonable extensional direction during the time of emplacement would be 110° . Using the average dip of 80° for dikes and normal faults in the Lagarfljót region and an oblique angle of 5° (based on the current spreading direction of 105°), the SS/N ratio would be 0.015 (Figure 31) (Einarsson, 2008). Such a low ratio does not fit with the field observations. This implies either the obliquity angle is incorrect or more likely, this is not the method of formation of the strike-slip faults.

Though it is currently not possible to estimate Tertiary spreading directions, an upper limit can be estimated. An angle of 30° , equivalent to the obliquity of the present day Reykjanes Ridge, results in a SS/N ratio of 0.1. This demonstrates that at most the cumulative net displacement along strike-slip faults is 1/10th that of normal faults, and probably closer to 1/100th. This is in agreement with field results, that show a lack of gouge or significant offset along any of the strike-slip fault zones. However based on the spreading and extension vectors, left-lateral faults would be expected. Using 115° for a horizontal extension direction, which could also be valid based on changing plate motions with time, right-lateral faults would be produced. The uncertainty of this relationship means strain partitioning to form strike-slip faults cannot be ruled out.

Another part of this hypothesis that does not hold up is the requirement that the two sets of faults are parallel. The difference in strike between the N-S strike-slip faults and the NE-SW normal faults shows they are not parallel. Cross-cutting relationships show that the NE-trending faults came after the strike-slip faults. However, there is a component of N-S normal faults that are observed in the study area as well (Figure 18). It is possible these are related to the N-S strike-slip faults via a strain partitioning model. It must be said that this discussion does not take into account any sort of rotation. According to the Nuvel-1A model of plate motion, rotation speed between the North American and Eurasian plates is 0.21° per million years over the last few million years (Demets et al., 1994, Einarsson, 2008). It is therefore unlikely that large-scale tectonic rotations have affected the Lagarfljót area, but it is possible that smaller-scale block rotations have occurred in the area to accommodate the propagating NVZ.

6.2.4 Block rotation via a propagating rift

Rift propagation in hotspot locations has been identified as a major process in building oceanic spreading centers (Hey et al., 2010; Hey, 1980). In Iceland, GPS data indicates the EVZ is propagating southwards (Lafemina, 2005), while the NVZ is widely considered to be propagating northwards as well (Einarsson, 2008; Karson, 2013). Studies in the Afar region of Africa show that propagating rifts can lead to rotation of crustal blocks that are caught



Esri, DeLorme, GEBCO, NOAA, NGDC, and other contributors

Figure 32. Figure showing strike-slip faulting in Iceland. The transform zones are outlined in blue. Black lines indicate the current rift boundaries. Orange lines are “psuedofaults” which delineate new crust created in the wake of the propagating rift. A net spreading difference between the tip of the rift and segments further along it leads to rotation of crustal blocks. This rotation is accommodated via a bookshelf type faulting mechanism, indicated in the figure above. Red lines indicate identified strike-slip faults, with SOS indicated where variance in along-strike spreading has been documented in the EVZ (Lafemina et al., 2005)

between adjacent segments of the ridge (Muluneh et al., 2013; Tapponnier & Armijo, 1991), in a style similar to that outlined previously by Greene et al. (2004). These block rotations are accommodated by bookshelf faulting along faults transverse to the overall shear direction. The Easter microplate is also a locality where rotation is accommodated by slip along its margins (Schouten et al., 1993)

A hypothesis relates to the idea of spreading along a propagating rift segment. As a rift propagates away from a central hotspot, there is a net difference in the spreading rate at the tip of the rift compared to locations closer to the hotspot (Muller et al., 1998; Scheiber-Enslin et al., 2011). Segments closer to the hotspot are closer to the magma supply, display more volcanism, and thus take up more of the overall spreading motion. The tip of the rift is relatively magma poor, and spreading is occurring at a much slower pace. This is reflected in 'pseudofaults' that define a v-shaped unconformity of younger lavas erupted on older deposits (Figure 32)(Hey, 1980). A difference in spreading rate along the ridge axis, could lead to rotation of crustal blocks on either side of the plate boundary. In the NVZ this would correlate with clockwise rotation of blocks to the west and counterclockwise rotation to the east (Figure 32). This rotation would need to be accommodated by internal deformation of crustal blocks. A method of bookshelf style faulting is proposed, which is analogous to an E-W left-lateral shear zone that is accommodated by slip on N-S right-lateral strike-slip faults. Slip is induced as the individual blocks rotate counterclockwise from N-S to NW-SE (Figure 32). This could explain the presence of strike-slip faulting in the Lagarfljót region that are found in N-S and NW-SE orientations. In a similar study conducted 40 km to the west, dextral strike-slip faults oriented at 30° were found to be cut by normal faults trending 45° (Chutas et al., 2006).

It is hard to constrain the absolute timing of the strike-slip faulting, and to relate it to the position of the propagating ridge. Based on cross cutting relationships and field evidence, the strike-slip faults seem to have been active prior to the injection of dikes and normal faulting, but after the Thingmuli system became dormant. One thing that is not clear is how the strike-slip faulting is related to the position of the rift. Is there an area a certain distance from the axis

where these faults are active? How does activity vary along the length of the axis? A clue may be a right-lateral strike-slip fault that was discovered in Kárahnjúkar 40 km to the west of the study area and 40 km east of the active rift zone. This fault was shown to be cutting Quaternary hyaloclastites, indicating this area may have been active within the past 2 million years (Chutas et al., 2006).

Enigmatic rift-parallel strike-slip faults are not well understood, and play a role in the tectonic development of Iceland. Moving forward, it is necessary to identify and study these features in detail in order to better understand rift propagation processes and rift hotspot interactions.

7. Conclusions

A comprehensive mapping and kinematic analysis carried out over the Lagarfljót region revealed a complicated history of deformation. N-S dikes and lavas related to the Thingmuli volcanic system were emplaced and subsequently tilted to the west. A component of N-S normal faulting also associated with the fissure swarm is present as well. The region then developed a flexure zone tilting some lavas up to 25°. This was likely related to a newly initiated or increasingly active rift basin around ~8 Ma.

Between 4 and 8 million years ago, N-S right-lateral strike-slip faults formed. No evidence exists to suggest these faults are related to an abandoned transform zone or to transform accommodation of adjacent fissure swarms, like those seen today. Oblique spreading is a possible explanation, but the expected structural relationships are not apparent. These faults are thus thought to be related to the regional context of a propagating ridge. Counterclockwise rotation of individual blocks accommodating differences in spreading rates along the ridge could give rise to the faults observed today. A series of NE-SW trending dikes and normal faults cut the strike-slip faults, and could be related to rift relocation. Continued study of this area, including dating and paleomagnetic work, will greatly enhance our understanding of these and other processes related to ridge hotspot interactions.

Appendix

RECORDED DATA

Faults

Waypoint	Structure	Strike	Dip	Rake	Plunge	Direction	Width (m)
394	F	350	90	160			1
395	F	355	90	160			1
403	F	210	75				8
411	F	20	75	165			6
412	F	5	70				4
419	F	350	90				3
419	F	170	90				3
421	F	0					3
442	F	340	90				3
444	F	0	70				3
457	F	60	90				2
458	F	510	80				2
459	F	110	80				2
460	F	345	80				2
461	F	340	80	-15			1.5
463	F	150	80				1
470	F	160	90	0			1
478	F	10	80				1
480	F	160	65	-90			1
481	F	135	65				1
490	F	355	90				1
492	F	205	80				1
498	F	330	80				1
502	F	330	80				1
527	F	0	75				1
532	F	150	70				1
533	F	9	0				1
533	F	65	65				1
536	F	25	80				1
537	F	20	80				1
539	F	5	65				1
545	F	15	68				0.8
547	F	235	65				0.8
550	F	25	90		DD		0.8

551	F	15	85				0.7
561	F	345	90				0.7
566	F	300	85		45	s	0.7
567	F	355	80				0.5
568	F	350	80				0.5
569	F	20	80		DD		0.5
571	F	315	70				0.5
572	F	340	55				0.5
577	F	10	90				0.5
590	F	5	85				0.4
602	F	340	80				0.4
609	F	345	80				0.3
636	F	32	65				0.3
638	F	355	60				0.2
642	F	175	70				0.2
647	F	35	74				0.2
648	F	1	83				0.2
673	F	0	76		45	N	0.08
683	F	22	86				0.05
684	F	180	77				
689	F	330	85				70.33
690	F	10	80				
719	F	0	77				
741	F	330	67		60	SE	
745	F	45	65		90		
750	F	200	70		90		
762	F	358	90				
764	F	359	90				
765	F	340	65				
770	F	179	76		90		
775	F	190	83				
775	F	193	85				
			76.954				

Fault Planes

Waypoint	Structure	Strike	Dip	Rake	Plunge	Direction
401	FP	344	88	-20		
401	FP	330	72	-20		
401	FP	348	79	0		
401	FP	143	66	25		
402	FP	350	70	-160		
402	FP	175	70	-80		
411	FP	55	85	155		
411	FP	55	80	155		
411	FP	45	50	160		
412	FP	345	90	-90		
412	FP	330	90	20		
412	FP	310	90	180		
415	FP	210	90	-170		
415	FP	237	85	-165		
415	FP	230	80	-165		
415	FP	250	75	-160		
415	FP	235	85	-155		
415	FP	235	85	-155		
415	FP	225	90	-155		
415	FP	350	80	-75		
415	FP	355	80	-70		
415	FP	205	80	15		
415	FP	0	70	155		
415	FP	10	70	160		
415	FP	0	70	160		
415	FP	355	75	160		
415	FP	355	75	165		
416	FP	196	57	-135		
416	FP	176	65	-130		
416	FP	150	68	-130		
416	FP	162	75	-130		
416	FP	191	65	-125		
416	FP	178	58	-115		
416	FP	204	72	-110		
416	FP	358	55	-110		
416	FP	220	90	-105		

416	FP	216	83	-105		
416	FP	212	74	-100		
416	FP	4	49	-100		
416	FP	45	61	-85		
416	FP	34	70	-85		
418	FP	5	55	55		
418	FP	5	55	65		
418	FP	8	58	70		
419	FP	190	90	-150		
419	FP	0	75	-150		
419	FP	170	80	-145		
419	FP	282	85	135		
419	FP	290	90	140		
419	FP	325	90	155		
421	FP	10	89		0	
421	FP	194	78		10	S
421	FP	9	85		10	S
421	FP	330	78		15	N
421	FP	2	85		15	S
421	FP	17	56		90	
421	FP	354	57	-100		
421	FP	220	85	90		
421	FP	305	65	90		
421	FP	5	87	155		
439	FP	10	80	140		
439	FP	5	90	145		
445	FP	355	90	-165		
445	FP	0	70	170		
445	FP	170	85	170		
456	FP	155	60	-105		
461	FP	325	90	-15		
472	FP	184	90	-100		
475	FP	10	85		30	N
481	FP	140	65	-90		
481	FP	130	65	-90		
491	FP	250	80	170		
494	FP	350	75	-120		
520	FP	25	80		15	N

520	FP	355	75		20	N
520	FP	175	75		40	N
527	FP	5	75	100		
534	FP	180	85	5		
534	FP	175	80	10		
534	FP	185	80	10		
541	FP	210	75	-90		
541	FP	240	65	-76		
544	FP	20	90	-90		
545	FP	10	80	-90		
554	FP	355	70	-100		
554	FP	355	85	-90		
555	FP	335	70	90		
556	FP	355	75	-10		
556	FP	345	85	-10		
558	FP	0	65		10	N
560	FP	205	55		90	
562	FP	350	80	-75		
568	FP	350	80	-45		
570	FP	210	85	-160		
572	FP	340	55	-90		
573	FP	20	80	-165		
574	FP	345	90	-170		
575	FP	20	65	-90		
577	FP	220	75		5	SW
577	FP	30	84	-170		
577	FP	95	80	-170		
577	FP	200	80	-160		
577	FP	340	85	-10		
578	FP	225	75		10	N
578	FP	204	87	-173		
578	FP	205	85	-170		
578	FP	28	85	165		
579	FP	40	80		5	N
579	FP	23	85	-175		
579	FP	25	80	150		
579	FP	40	85	165		
580	FP	335	80	35		

580	FP	15	80	125		
580	FP	38	82	150		
580	FP	40	78	155		
581	FP	315	85	20		
583	FP	183	87	-90		
583	FP	200	87	-70		
584	FP	330	90	-80		
586	FP	210	80	-90		
588	FP	20	80		10	N
589	FP	200	85		5	N
589	FP	195	85		5	S
589	FP	20	65	-90		
591	FP	180	85	5		
592	FP	60	85		90	
592	FP	330	85		90	
592	FP	320	80	-80		
594	FP	5	65		90	
597	FP	35	25	-20		
602	FP	240	85		45	SE
602	FP	25	60		50	NE
602	FP	356	72		80	N
603	FP	60	80		20	E
603	FP	85	82		55	W
603	FP	170	80		60	S
603	FP	120	68		75	W
604	FP	305	80		45	NW
604	FP	300	88		50	NW
605	FP	22	70	-179		
605	FP	20	80	-165		
607	FP	340	75		90	
607	FP	290	87	-170		
607	FP	345	80	-170		
607	FP	348	81	-135		
608	FP	350	78	-165		
610	FP	70	45		75	E
610	FP	0	56		85	S
611	FP	350	63	-90		
612	FP	340	65	-80		

618	FP	320	87	-170		
619	FP	293	83		45	NW
619	FP	300	85	-45		
619	FP	162	80	-40		
620	FP	315	85		15	NW
621	FP	50	85		75	SW
621	FP	165	47		90	
621	FP	20	87		90	
621	FP	174	50		90	
621	FP	181	73	-100		
622	FP	190	85		20	S
622	FP	60	86		60	N
622	FP	168	78		60	S
622	FP	320	87	-170		
623	FP	168	78		60	S
623	FP	150	80		90	
624	FP	150	87		20	S
624	FP	330	79	-165		
624	FP	126	85	-155		
625	FP	333	70		15	W
625	FP	266	81		65	W
625	FP	284	75		70	W
625	FP	267	80		80	W
627	FP	184	48		90	
627	FP	176	65		90	
627	FP	172	69		90	
627	FP	145	55	-90		
627	FP	189	53	-80		
627	FP	330	75			
628	FP	14	60		90	
628	FP	346	85		90	
631	FP	190	68		48	N
638	FP	155	73		90	
638	FP	176	60		90	
638	FP	355	60	-80		
640	FP	3	90		30	S
640	FP	10	87		35	S
640	FP	165	77		80	N

640	FP	5	90		90	
641	FP	125	86		18	S
641	FP	156	85		20	S
641	FP	350	64		25	S
643	FP	165	85	175		
644	FP	166	83		10	N
645	FP	5	87		5	N
648	FP	353	69	160		
648	FP	355	79	165		
649	FP	10	78		15	N
652	FP	32	64	-90		
652	FP	10	63	-90		
652	FP	235	72	-90		
654	FP	198	83		75	N
654	FP	215	81		90	
654	FP	213	80		90	
655	FP	115	71		90	
655	FP	46	80		90	
655	FP	186	56	-90		
656	FP	130	90		80	NW
656	FP	166	84	-45		
656	FP	165	81	-40		
656	FP	159	87	-30		
660	FP	0	61		35	N
663	FP	355	84		90	
664	FP	171	65		90	
665	FP	242	85		15	S
665	FP	215	85		20	S
665	FP	330	80		20	S
665	FP	200	83		45	S
665	FP	40	66		90	
666	FP	205	81		70	N
666	FP	346	78		75	N
674	FP	213	87		30	NE
674	FP	170	84		90	
674	FP	175	80		90	
686	FP	36	50		90	
687	FP	178	85		90	

687	FP	55	44		90	
689	FP	161	81		45	N
693	FP	178	89		25	N
699	FP	55	87		50	N
700	FP	350	80		45	N
702	FP	0	65		30	N
702	FP	290	75		60	N
703	FP	356	78		15	N
705	FP	336	70		10	N
706	FP	85	80		90	
706	FP	85	90		90	
707	FP	330	85	175		
708	FP	320	74	-165		
708	FP	255	85	-90		
709	FP	310	90		10	S
709	FP	315	90		10	N
710	FP	315	90		10	N
718	FP	200	85		90	
721	FP	355	70		90	
722	FP	357	62	-90		
726	FP	175	90		5	N
726	FP	215	80		45	S
727	FP	215	80		45	S
728	FP	200	67	-90		
731	FP	345	87		10	N
731	FP	355	68		35	N
738	FP	300	85	165		
738	FP	305	87	170		
739	FP	186	75		20	N
739	FP	186	75	-40		
740	FP	15	87		5	W
740	FP	39	79		10	SW
740	FP	23	90		20	SW
740	FP	181	84	-175		
740	FP	20	80	-170		
740	FP	21	80	-155		
740	FP	358	80	165		
742	FP	330	73		10	NW

742	FP	345	80		15	N
742	FP	310	90		15	NW
742	FP	34	80		15	NE
742	FP	4	75		20	S
742	FP	175	89		20	N
742	FP	65	75		25	W
742	FP	295	85		25	NW
742	FP	350	76		35	N
742	FP	192	85		40	N
742	FP	198	65		40	N
742	FP	340	80		45	N
742	FP	223	77		45	NE
742	FP	78	75		50	E
742	FP	4	60		55	S
742	FP	242	70		75	W
742	FP	350	72	-175		
742	FP	325	76	-170		
742	FP	355	75	45		
742	FP	11	76	165		
743	FP	310	87		10	S
743	FP	285	83	45		
743	FP	340	80	160		
743	FP	350	74	160		
746	FP	20	61		35	N
746	FP	340	77		35	N
746	FP	358	89		45	N
746	FP	356	89		45	N
746	FP	166	84		45	N
746	FP	50	71		48	N
746	FP	30	89		60	N
747	FP	340	69		90	
749	FP	22	87		10	SW
749	FP	350	80		25	N
749	FP	250	40		60	NE
749	FP	350	80		70	N
749	FP	320	59		80	NW
751	FP	195	86	90		
752	FP	5	76		10	S

752	FP	25	72		10	S
752	FP	15	81		10	S
752	FP	10	87		10	N
753	FP	0	85		10	N
753	FP	350	82		15	N
753	FP	155	89		20	S
755	FP	67	89		15	E
756	FP	230	54	90		
756	FP	348	69	120		
756	FP	90	80	120		
756	FP	348	84	145		
757	FP	153	80	-55		
757	FP	160	75	-45		
757	FP	158	75	-45		
758	FP	25	87		5	N
758	FP	350	73		5	S
758	FP	188	83		10	N
758	FP	291	70		20	E
758	FP	340	90	-170		
758	FP	0	75	-90		
758	FP	355	76	170		
759	FP	42	88		0	
759	FP	220	88		5	N
759	FP	220	87		10	N
759	FP	325	60		10	S
759	FP	35	85		10	N
759	FP	10	85		15	N
759	FP	319	70		20	SE
759	FP	46	65		20	SW
759	FP	299	71		20	W
759	FP	290	90	155		
759	FP	300	45	160		
759	FP	295	83	175		
759	FP	305	81	175		
759	FP	295	85	175		
759	FP	300	85	180		
760	FP	210	55		90	
760	FP	200	65	-90		

778	FP	30	70		90	
-----	----	----	----	--	----	--

All Dikes

Waypoint	Structure	Strike	Dip	Width (m)
391	D	12	69	0.3
392	D	25	90	0.4
393	D	6	86	0.4
396	D	165	75	0.5
398	D	10	90	0.5
399	D	5	90	0.5
404	D	355	85	0.5
407	D	25	83	0.75
409	DF	0	55	3
410	D	20	72	0.75
413	DF	163	74	3
420	D	20	82	0.75
428	D	183	75	0.75
429	D	185	55	0.75
430	D	140	73	0.75
433	D	25	61	0.8
433	D	38	55	0.8
433	D	6	58	0.8
434	D	355	80	1
435	D	40	80	1
436	DF	40	65	3
437	D	30	75	1
440	DF	355	80	3
441	DF	355	68	3
446	DF	21	65	3
447	D	15	69	1
448	DF	340	90	3
451	DF	15	70	3
452	D	355	90	1
453	D	161	67	1
454	DF	5	90	3

455	D	162	86	1
456	DF	165	55	3
459	D	358	90	1
462	D	345	90	1
465	D	335	40	1
466	D			1
468	DF	22	80	3
469	D	6	85	1
469	D	9	82	1
469	D	23	76	1
471	D	3	90	1
472	D	191	83	1
473	D	191	85	1
474	D	200	80	1
477	DF	10	90	3
481	D	140	65	1
482	D	30	90	1
483	D	0	90	1
485	DF	330	90	3
486	DF	190	80	3
487	DF	10	90	3
488	D	355	90	1
494	DF	345	80	3
496	DF	209	64	3.5
500	D	176	65	1
501	DF	5	85	4
503	D	0	90	1
504	D	155	90	1
505	DF	20	75	4
506	D	357	85	1
507	D	50	80	1
509	D	10	90	1
510	D	340	80	1
510	D	340	80	1
512	D	173	72	1
513	D	343	80	1
514	DF	0	90	4
516	D	4	80	1

516	D	54	90	1
517	D	170	80	1
518	DF	170	80	4
519	D	30	90	1
520	D	330	80	1
520	DF	30	90	4
521	DF	22	90	4
523	DF	212	85	4
524	D	18	90	1
525	DF	20	60	4
529	DF	0	90	4
530	DF	354	80	4
530	DF	6	80	4
530	DF	356	80	4
530	DF	350	80	4
531	D	20	80	1
534	DF	341	66	4.5
535	D	12	76	1.25
535	D	12	76	1.25
538	D	345	75	1.25
542	D	31	90	1.25
543	D	350	85	1.5
544	D	25	90	1.5
545	D	15	90	1.5
546	D	22	78	1.5
547	DF	215	66	4.5
548	DF	358	60	5
549	DF	10	80	5
551	D	15	85	1.5
551	D	320	90	1.5
552	D	190	50	1.5
553	D	340	70	1.5
556	D	185	80	1.5
557	D	10	80	1.5
559	D	338	75	1.5
565	DF	125	80	5
567	D	12	76	1.5
575	DF	20	65	5

576	D	28	78	1.75
587	D	20	85	2
587	D	10	85	2
587	D	15	85	2
589	DF	0	80	5
590	D	5	85	2
595	DF	20	80	6
598	DF	0	87	6
601	D	350	86	2
606	D	352	68	2
612	D	348	75	2
613	DF	20	75	6
621	DF	173	74	6
623	DF	190	80	7
626	D	162	84	2
627	DF	335	86	20
628	DF	171	86	
630	DF	343	72	
631	DF	190	68	
632	D	221	87	2
634	D	330	85	2
634	D	33	86	2
640	DF	165	77	
646	DF	357	72	
650	DF	230	87	
652	DF	14	60	
661	DF	0	85	
663	DF	355	84	
664	DF	348	69	
665	D	215	87	2
667	DF	355	90	
668	D	357	90	2
669	D	175	74	2
670	D	200	72	2
671	DF	25	85	
672	D	115	72	2
674	D	194	80	2
675	D	170	80	2

678	D	160	74	2
679	D	3	87	2
680	DF	335	90	
681	D	189	85	2
682	D	191	90	2
685	D	340	83	2
689	DF	185	89	
691	D	35	66	2
694	D	345	89	2
695	D	335	90	2
696	D	3	71	2
697	D	20	90	2
701	DF	8	54	
701	DF	5	70	
704	DF	155	82	
712	DF		205	
714	DF	21	80	
715	D	20	89	2
716	D	20	85	2
717	D	205	85	2
718	DF	200	85	
724	D	30	90	2
725	D	40	90	2
730	DF	185	678	
732	D	180	75	2
732	D	20	65	2.5
734	DF	171	49	
734	DF	170	75	
754	D	345	45	3
766	DF	295	75	
767	DF	10	90	
768	D	25	80	3
769	D	23	85	3
771	DF	355	80	
773	D	350	90	3
776	D	180	85	3
777	DF	20	65	

Waypoint	Structure	Strike	Dip
585	L	30	5
587	L		
614	L	190	19
616	L	195	20
624	L	10	8
635	L	170	9
647	L	180	8
662	L	190	10
686	L	10	24
687	L	160	25
692	L	171	20
699	L	210	20
704	L		16
713	L		
729	L		10
736	L		9
745	L		10
761	L		10
774	L		10

Hafursa

Waypoint	Structure	Strike	Dip	Rake	Plunge	Direction	Width (m)
618	FP	320	87	-170			
619	FP	162	80	-40			
619	FP	300	85	-45			
619	FP	293	83		45	NW	
620	FP	315	85		15	NW	
621	DF	173	74				2.5
621	FP	181	73	-100			
621	FP	165	47		90		
621	FP	20	87		90		
621	FP	50	85		75	SW	
621	FP	174	50		90		
622	FP	320	87	-170			
622	FP	60	86		60	N	
622	FP	168	78		60	S	
622	FP	190	85		20	S	
623	DF	190	80				
623	FP	168	78		60	S	
623	FP	150	80		90		
624	FP	126	85	-155			
624	FP	330	79	-165			
624	FP	150	87		20	S	
624	L	10	8				
625	FP	267	80		80	W	
625	FP	266	81		65	W	
625	FP	284	75		70	W	
625	FP	333	70		15	W	
626	D	162	84				
627	DF	335	86				
627	FP	189	53	-80			
627	FP	145	55	-90			
627	FP	184	48		90		
627	FP	176	65		90		
627	FP	172	69		90		
627	FP	330	75				
628	DF	171	86				0.8

628	FP	14	60		90		
628	FP	346	85		90		0.2
629							
630	DF	343	72				
631	DF	190	68				
631	FP	190	68		48	N	2
632	D	221	87				1.5
633							
634	D	330	85				5
634	D	33	86				5
635	L	170	9				
636	F	32	65				1
637							
638	F	355	60				1
638	FP	355	60	-80			
638	FP	155	73		90		
638	FP	176	60		90		
639							
640	DF	165	77				1
640	FP	10	87		35	S	
640	FP	3	90		30	S	
640	FP	5	90		90		
640	FP	165	77		80	N	
641	FP	156	85		20	S	
641	FP	125	86		18	S	
641	FP	350	64		25	S	
642	F	175	70				
643	FP	165	85	175			
644	FP	166	83		10	N	
645	FP	5	87		5	N	
738	FP	305	87	170			
738	FP	300	85	165			
739	FP	186	75	-40			
739	FP	186	75		20	N	
740	FP	358	80	165			
740	FP	21	80	-155			
740	FP	20	80	-170			
740	FP	181	84	-175			

740	FP	23	90		20	SW	
740	FP	39	79		10	SW	
740	FP	15	87		5	W	
741	F	330	67		60	SE	
742	FP	11	76	165			
742	FP	355	75	45			
742	FP	325	76	-170			
742	FP	350	72	-175			
742	FP	4	60		55	S	
742	FP	340	80		45	N	
742	FP	345	80		15	N	
742	FP	65	75		25	W	
742	FP	310	90		15	NW	
742	FP	330	73		10	NW	
742	FP	4	75		20	S	
742	FP	295	85		25	NW	
742	FP	192	85		40	N	
742	FP	198	65		40	N	
742	FP	242	70		75	W	
742	FP	34	80		15	NE	
742	FP	78	75		50	E	
742	FP	223	77		45	NE	
742	FP	350	76		35	N	
742	FP	175	89		20	N	
743	FP	340	80	160			
743	FP	350	74	160			
743	FP	285	83	45			
743	FP	310	87		10	S	
744							
745	F	45	65		90		8
745	L		10				

References

- Abbate, E., Passerini, P., Zan, L. (1995). Strike-slip faults in a rift area: a transect in the Afar Triangle, East Africa. *Tectonophysics*, 241(1-2), 67–97.
- Allmendinger, R. W. (2012). FaultKin.
- Allmendinger, R.W., Gephart, J.W., Marrett, R.A. (1989). Notes on fault slip analysis. *Quantitative Interpretation of Joints and Faults*. GSA Short Course.
- Arnadóttir, T., Lund, B., Jiang, W., Geirsson, H., Björnsson, H., Einarsson, P., Sigurdsson, T. (2009). Glacial rebound and plate spreading: results from the first countrywide GPS observations in Iceland. *Geophysical Journal International*, 177(2), 691-716.
- Carmichael, I. S. E. (1964). The Petrology of Thingmuli , a Tertiary Volcano in Eastern Iceland. *Journal of Petrology*, 5, 434–460.
- Chutas, L.A. (2006). Rift-Parallel Strike-Slip Faulting in the Kárahnjúkar area of Eastern Iceland. MS Thesis, Duke University, 1-148
- Clifton, A. E., Kattenhorn, S. A. (2006). Structural architecture of a highly oblique divergent plate boundary segment. *Tectonophysics*, 419(1-4), 27–40.
- DeMets, C., Gordon, R., Argus, D., Stein, S. (1994). Effect of recent revisions to the geomagnetic reversal time scale on estimates of current plate motions. *Geophysical research letters*, 21(20), 2191–2194.
- Einarsson, P. (1991). Earthquakes and present-day tectonism in Iceland. *Tectonophysics*, 189, 261–279.
- Einarsson, P. (2008). Plate boundaries, rifts and transforms in Iceland. *Jökull*, 58, 35–58.
- Forslund, T., Gudmundsson, A. (1992). Structure of Tertiary and Pleistocene Normal Faults in Iceland. *Tectonics*, 11(1), 57–68.
- Garcia, S., Arnaud, N. O., Angelier, J. (2003). Rift jump process in Northern Iceland since 10 Ma from $^{40}\text{Ar} / ^{39}\text{Ar}$ geochronology, *Earth and Planetary Science Letters*, 214, 529–544.
- Green, R., White, R., Greenfield, T. (2013). Motion in the north Iceland volcanic rift zone accommodated by bookshelf faulting. *Nature Geoscience*. 7, 29-33.

- Grant, J. V., Kattenhorn, S. A. (2004). Evolution of vertical faults at an extensional plate boundary, southwest Iceland. *Journal of Structural Geology*, 26(3), 537–557.
- Gudmundsson, A. (1996). Stress fields controlling strike-slip faulting in Iceland. *Physics and Chemistry of the Earth*, 2(4), 261–265.
- Gudmundsson, A. (1978). Austurlandsvirkun- Mulavirkjun. Framkonnun a jardfraedi Mula og umhverfis. (The geology of Muli and its surroundings). National Energy Authority of Iceland, Report OS-ROD 7818. 50pp. and maps (in Icelandic).
- Gudmundsson, A. (1984). Tectonic aspects of dykes in northwestern Iceland. *Jökull*, 34, 81-96
- Hardarson, B., Fitton, J. (1997). Rift relocation—a geochemical and geochronological investigation of a palaeo-rift in northwest Iceland. *Earth and Planetary Science Letters*, 153(97), 181–196.
- Hards, V., Kempton, P., Thompson, R., Greenwood, P. (2000). The magmatic evolution of the Snæfell volcanic centre; an example of volcanism during incipient rifting in Iceland. *Journal of Volcanology and Geothermal Research*, 99(1-4), 97–121.
- Helgason, J. (1984). Frequent shifts of the volcanic zone in Iceland. *Geology*, 12, 212–216.
- Hey, R., Martinez, F., Höskuldsson, Á., Benediktsdóttir, Á. (2010). Propagating rift model for the V-shaped ridges south of Iceland. *Geochemistry, Geophysics, Geosystems*, 11(3), 1-24.
- Hey, R. (1980). Propagating rifts on midocean ridges. *Journal of Geophysical Research*, 85(80), 3647–3658.
- Hjartardóttir, Á. R., Einarsson, P. (2011). The Kverkfjöll fissure swarm and the eastern boundary of the Northern Volcanic Rift Zone, Iceland. *Bulletin of Volcanology*, 74(1), 143–162.
- Jóhannesson, H., K. Sæmundsson (2009). Geological map of Iceland. Institute of Natural History, Reykjavík (1st edition).
- Kamb, W.B. (1959). Ice petrofabric observations from Blue Glacier, Washington in relation to theory and experiment. *Journal of Geophysical Research*, 64, 1891-1909.
- Karson, J. (2013). Rift to drift transition at volcanic rifts and rifted margins: lessons from Iceland. American Geophysical Union, Fall Meeting, abstract #T205-182-11
- Kristjánsson, L., Gudmundsson, A. (2005). Stratigraphy and paleomagnetism of lava sequences in the Suðurdalur area, Fljótisdalur, Eastern Iceland. *Jökull*, 55, 17–32.

- LaFemina, P. C., Dixon, T. H., Malservisi, R., Árnadóttir, T., Sturkell, E., Sigmundsson, F., Einarsson, P. (2005). Geodetic GPS measurements in south Iceland: Strain accumulation and partitioning in a propagating ridge system. *Journal of Geophysical Research*, 110 (B11405).
- Marrett, R., Allmendinger, R. (1990). Kinematic analysis of fault-slip data. *Journal of Structural Geology*, 12(8), 973–986.
- Martin, E., Paquette, J. L., Bosse, V., Ruffet, G., Tiepolo, M., Sigmarrsson, O. (2011). Geodynamics of rift–plume interaction in Iceland as constrained by new $^{40}\text{Ar}/^{39}\text{Ar}$ and in situ U–Pb zircon ages. *Earth and Planetary Science Letters*, 311(1-2), 28–38.
- McDougall, I., Watkins, N. D., Kristjánsson, L. (1976). Geochronology and paleomagnetism of a miocene-pliocene lava sequence at Bessastadaa, Eastern Iceland. *American Journal of Science*, 276, 1078–1095.
- McDougall, I., Watkins, N., Walker, G. P. L., Kristjánsson, L. (1976). Potassium-argon and paleomagnetic analysis of Icelandic lava flows : Limits on the age of anomaly 5. *Journal of Geophysical Research*, 81(8), 1505–1512.
- Moorbath, S., Sigurdsson, H., Goodwin, R. (1968). K-Ar ages of the oldest exposed rocks in Iceland. *Earth and Planetary Science Letters*, 4, 197–205.
- Morgan, J., Kleinrock, M. (1991). Transform zone migration: implications of bookshelf faulting at oceanic and Icelandic propagating ridges. *Tectonics*, 10(5), 920–935.
- Müller, R., Roest, W., Royer, J. (1998). Asymmetric sea-floor spreading caused by ridge–plume interactions. *Nature*, 396, 455–460.
- Mulneh, A., Kidane, T., Rowland, J., Bachtadse, V. (2013). Counterclockwise block rotation linked to southward propagation and overlap of sub-aerial Red Sea Rift segments, Afar Depression: Insight from paleomagnetism. *Tectonophysics*, 593, 111–120.
- Nanfity, A., Karson, J.A. (2009). Complex Rift-Parallel, Strike-Slip Faulting in Iceland: Kinematic Analysis of the Gljúfurá Fault Zone. MS Thesis, Syracuse University, 1-61.
- Óskarsson, B. V., Riishuus, M. S. (2014). The mode of emplacement of Neogene flood basalts in eastern Iceland: Facies architecture and structure of simple aphyric basalt groups. *Journal of Volcanology and Geothermal Research*, 289, 170–192.

- Pálmason, G. (1973). Kinematics and heat flow in a volcanic rift zone, with application to Iceland. *Geophysical Journal International*, 33, 451–481.
- Paquet, F., Dauteuil, O., Hallot, E., Moreau, F. (2007). Tectonics and magma dynamics coupling in a dyke swarm of Iceland. *Journal of Structural Geology*, 29(9), 1477–1493.
- Passerini, P., Marcucci, M., Sguazzoni, G., Pecchioni, E. (1997). Longitudinal strike-slip faults in oceanic rifting : a mesostructural study from western to southeastern Iceland. *Tectonophysics*, 269, 65–89.
- Passerini, P., Marcucci, M., Sguazzoni, G. (1991). Strike-Slip faults parallel to crustal spreading axes: data from Iceland and the Afar Depression. *Terra Nova*, 3(6), 607–618.
- Petit, J. P. (1987). Criteria for the sense of movement on fault surfaces in brittle rocks. *Journal of Structural Geology*, 9(5/6), 597–608.
- Rubin, A., Pollard, D. (1988). Dike-induced faulting in rift zones of Iceland and Afar. *Geology*, 16, 413–417.
- Ryan, W.B.F., S.M. Carbotte, J.O. Coplan, S. O’Hara, A. Melkonian, R. Arko, R.A. Weissel, V. Ferrini, A. Goodwillie, F. Nitsche, J. Bonczkowski, and R. Zemsky (2009). Global multi-resolution topography synthesis. *Geochem. Geophys. Geosyst.*, 10, Q03014
- Saemundsson, K. (1974). Evolution of the Axial Rifting Zone in Northern Iceland and the Tjornes Fracture Zone. *Geologic Society of America Bulletin*, 85, 495-504.
- Scheiber-Enslin, S. E., LaFemina, P. C., Sturkell, E., Hooper, A. J., Webb, S. J. (2011). Geodetic investigation of plate spreading along a propagating ridge: the Eastern Volcanic Zone, Iceland. *Geophysical Journal International*, 187(3), 1175–1194.
- Scholz, C. (1987). Wear and gouge formation in brittle faulting. *Geology*, 15, 493–495.
- Schouten, H., Klitgord, K., Gallo, D. (1993). Edge driven microplate kinematics. *Journal of Geophysical Research*, 98, 6689–6701.
- Tapponnier, P., Armijo, R. (1990). Bookshelf faulting and horizontal block rotations between overlapping rifts in southern Afar. *Geophysical Research Letters*, 17(1), 1–4.
- Walker, G. P. L. (1958). Geology of the Reydarfjordur Area, Eastern Iceland. *Quarterly Journal of the Geological Society*, 114(1-4), 367–391.

Walker, G. P. L. (1974). The structure of Eastern Iceland. *Geodynamics of Iceland and the North Atlantic Area NATO Advanced Study Institutes*, 11, 177-188

Watkins, N., Walker, G. (1977). Magnetostratigraphy of Eastern Iceland. *American Journal of Science*, 277, 513-584

Woodcock, N. (1986). The role of strike-slip fault systems at plate boundaries. *Philosophical Transactions of the Royal Society of London*, 317, 13–29.

Vita

NAME OF AUTHOR: Keegan T. Runnals

PLACE OF BIRTH: Concord, NH

UNDERGRADUATE SCHOOLS ATTENDED:

Bates College, Lewiston ME

DEGREES AWARDED:

Bachelor of Science in Geology, 2011, Bates College, Lewiston, ME

AWARDS AND HONORS:

Syracuse University, Department of Earth Sciences Chair's Award, 2015

PROFESSIONAL EXPERIENCE:

BrandVerity, Analyst, January 2012 - June 2013

Syracuse University, Department of Earth Sciences, Teaching assistant for EAR 110, Dynamic Earth, Fall 2013

Syracuse University, Department of Earth Sciences, Teaching assistant for EAR 106, Geohazards and Natural Disasters, Spring 2014

Syracuse University, Department of Earth Sciences, Teaching assistant for EAR 333, Structural Geology, Fall 2014

Syracuse University, Department of Earth Sciences, Teaching assistant for EAR 225, Volcanoes and Earthquakes, Spring 2014